River flooding mechanisms and their changes in Europe revealed by explainable machine learning

Shijie Jiang[1], Emanuele Bevacqua[1], Jakob Zscheischler[1]

[1]Department of Computational Hydrosystems, Helmholtz Centre for Environmental Research, Leipzig, 04318, Germany

Correspondence to: Shijie Jiang (shijie.jiang@ufz.de)

Abstract. Climate change may systematically impact hydro-meteorological processes and their interactions, resulting in changes in flooding mechanisms. Identifying such changes is important for flood forecasting and projection. Currently, there is a lack of observational evidence regarding trends in flooding mechanisms in Europe, which requires reliable methods to disentangle emerging patterns from the complex interactions between flood drivers. ~~By using a novel explainable machine learning~~Recently, numerous studies have demonstrated the skill of machine learning (ML) for predictions in hydrology, e.g., for predicting river discharge based on its relationship with meteorological drivers. The relationship, if explained properly, may provide us with new insights into hydrological processes. Here, by using a novel explainable ML framework, combined with cluster analysis, we identify three primary patterns that drive 55,828 annual maximum discharge events in over a thousand European catchments. The patterns can be associated with three catchment-wide river flooding mechanisms: recent precipitation, antecedent precipitation (i.e., excessive soil moisture), and snowmelt. The results indicate that over half of the studied catchments are controlled by a combination of the above mechanisms, especially recent precipitation in combination with excessive soil moisture, which is the dominant mechanism in one-third of the catchments. Over the past 70 years, significant changes in the dominant flooding mechanisms have been detected within a number of European catchments. Generally, the number of snowmelt-induced floods has decreased significantly whereas floods driven by recent precipitation have increased. The detected changes in flooding mechanisms are consistent with the expected climate change responses, and we highlight the risks associated with the resulting impact on flooding seasonality and magnitude. Overall, the study ~~demonstrates the important role of explainable machine learning in uncovering complex and possibly non-linear~~offers a new perspective on understanding changes in weather and climate ~~extremes~~extreme events ~~and their drivers under climate change~~by using explainable ML and demonstrates the prospect of future scientific discoveries supported by artificial intelligence.

1 Introduction

River flooding is a pervasive natural hazard that regularly causes substantial economic, societal, and environmental damages worldwide (Merz et al., 2021; Tellman et al., 2021). With a warming atmosphere, flooding risk is projected to increase due to an intensification of the water cycle over large areas (Hirabayashi et al., 2013; Alfieri et al., 2017). For Europe, large-scale studies have revealed changes in flooding frequency, seasonality, and magnitude over the past decades, with considerable

variations across catchments (Alfieri et al., 2015; Blöschl et al., 2017; Hall and Blöschl, 2018; Blöschl et al., 2019; Bertola et al., 2020). The spatial inconsistency in these trends reflects differences in flood generating processes across the continent, which underscores the need for a better understanding of flood drivers (Keller et al., 2018).

In recent years, numerous studies have investigated river flooding mechanisms and some of them have provided European-scale assessments (e.g., Berghuijs et al., 2016; Berghuijs et al., 2019; Kemter et al., 2020; Bertola et al., 2021; Stein et al., 2021). Catchment-level floods can typically be attributed to the interaction of hydro-meteorological processes, such as extreme precipitation, soil moisture excess, and snowmelt (Merz and Blöschl, 2003; Tarasova et al., 2019). The dominant controlling

40 processes in catchments were usually identified either qualitatively by comparing the observed flood trends with the contemporaneous changes in flooding drivers (e.g., Blöschl et al., 2017; Blöschl et al., 2019) or quantitatively by calculating the seasonal similarities between flood events and potential drivers (e.g., Berghuijs et al., 2016; Berghuijs et al., 2019). Such analyses revealed the dominant flood generating processes at a catchment level, improving the understanding of climate change effects on flooding magnitude and timing. However, the methods ~~either~~often implicitly ~~assumed~~assume temporally consistent

45 flood processes within a catchment (Merz et al., 2012), ~~or were limited in the little interannual variability of seasonality statistics ,~~making it difficult to detect possible changes in flooding mechanisms themselves in a warming climate.

Flooding mechanisms that dominate one catchment are not always immutable but might shift over time, particularly in light of climate change (Hall et al., 2014). For example, increasing temperatures can affect snow dynamics in cold regions and result

50 in more rainfall extremes, which could make snowmelt-dominated catchments more susceptible to extreme rainfall and thereby alter the regional flood seasonality and magnitudes (Vormoor et al., 2016; Davenport et al., 2020; Rottler et al., 2021). Therefore, a systematic investigation of the changes in flooding mechanisms is necessary. Yet few studies have been able to quantify how the mechanisms evolved over time on a continental scale in Europe. The identification of specific trends in flooding mechanisms requires a comprehensive understanding of hydrological processes underlying individual events (Stein

55 et al., 2020). Currently available studies that attempted to classify river flooding processes on an event basis typically rely on multicriteria approaches, which require predefining thresholds for a variety of hydrometeorological indicators, such as the storm duration and snowmelt amount (e.g., Nied et al., 2014; Stein et al., 2021). Using a multicriteria approach, Kemter et al. (2020) identified the flooding mechanisms in Europe by classifying approximately 174,000 flood peaks and revealed their trends over the past 50 years. Likewise, Stein et al. (2020) analyzed flood events over 4,155 catchments worldwide and

60 classified them into five flood-generating processes. Despite the computational efficiency of using multicriteria approaches, the obtained insights are often dependent on the careful choice of indicators and thresholds. For example, in some cases, a small change in a threshold value modifies the classification, potentially compromising the robustness of the results (Sikorska et al., 2015). Alternatively, some studies grouped flood events by inductive analyses, which adopted clustering methods to obtain flood types from hydrometeorological indicators (e.g., Turkington et al., 2016; Keller et al., 2018). However, the chosen

65 indicators (e.g., snow-covered area, day of occurrence, and 95th percentile of spatial precipitation distribution) did not

unambiguously indicate flooding mechanisms since they were not indicative of the causal contribution of flood drivers to peak discharges (Tarasova et al., 2019).

An effective way to identify flooding mechanisms for individual flood events is to quantify the contribution of possible drivers to its occurrence, which involves uncovering the implicit connections that may exist between flood events and meteorological observations. This can be achieved by machine learning (ML), which has been receiving increasing attention in Earth and climate sciences for its remarkable ability to identify and generalize predictive relations with a high-level abstract representation (Reichstein et al., 2019; Yu and Ma, 2021). In hydrology particularly, one excellent example is the prevalence of long short-term memory (LSTM) neural networks (Kratzert et al., 2018; Shen, 2018), which have been demonstrated to learn patterns conceptually consistent with qualitative understandings of how hydrological systems work as opposed to simply trivial coincidences (Kratzert et al., 2019a). Extraction of captured patterns from "black-box" ML models with feature attribution techniques (i.e., ML interpretations) may lead to theoretical advances and can assist in making new scientific discoveries, as recently demonstrated for climate, ocean, and weather applications (e.g., Barnes et al., 2020; Toms et al., 2020; Labe and Barnes, 2021), including the identification of flooding mechanisms (Jiang et al., 2022).

In this study, we will revisit flooding mechanisms in Europe over the period 1950–2020 by using an improved framework based on the explainable ML methods developed by Jiang et al. (2022) and compare the results with existing studies. We base the analysis on over 1,000 catchments and the only dynamic information necessary for the analysis is precipitation, temperature, and streamflow. These three variables can be readily measured, thereby reducing the reliance on possibly uncertain estimations of fluxes and state variables (such as soil moisture). The combination of supervised learning-based feature attribution and unsupervised learning-based cluster analysis reduces subjectivity and uncertainty for the selection of appropriate indicators and thresholds in the categorization of flood drivers. Moreover, taking an event-level perspective, we quantify the changes that occurred in these mechanisms in the past seven decades, and discuss the possible reasons and implications of the detected changes. Overall, the study contributes to a better understanding of river flood risk and how it is affected by climate change and illustrates how explainable ML can advance knowledge about the Earth system.

2 Data and methodologies

2.1 Data

The study considers 1,077 catchments in the domain of Europe (Fig. 1a) based on the data availability of daily river discharge observations from the Global Runoff Data Centre (GRDC) dataset (https://www.bafg.de/GRDC). We restricted our analysis to catchments having an area of 10,000 km² or less to exclude overly large catchments and having a minimum of 20 years of discharge records within 1950–2020 to ensure sufficient samples to train the ML models. The catchment areas range between 8 km² and 10,000 km² — very large catchments, where the effect of spatial heterogeneity of flood drivers tends to be

substantial, were not considered. For those catchments, the sample size of daily discharge records ranges from 7,300 to 25,753, with a median of 20,455. Overall, the selected catchments encompass a variety of geographical and climatic conditions, as illustrated by the catchment distributions in terms of average elevation, average slope, catchment size, aridity index, snowfall fraction, and flood mean date (FigureFig. 1). The elevation, slope, and size were derived from the Global Streamflow Indices and Metadata Archive (GSIM) (Do et al., 2018), the aridity index and snowfall fraction were calculated from the catchment-averaged precipitation and temperature described later. In the study, floods are defined as the annual maxima (peaks) of river discharge time series in line with common practices (e.g., Blöschl et al., 2017; Blöschl et al., 2019). The above properties will also be used to discuss their relevance to the catchment-level dominant flood mechanisms.

We considered precipitation, temperature, and day length as input variables of the ML models. Using the 0.1° daily gridded precipitation and mean surface temperature data from the E-OBS dataset (version 23.1e) (Haylock et al., 2008), we calculated the catchment-averaged time series of these variables based on area-weighted averages of the data pixels within the catchment boundary. The weight of each pixel was determined by the fraction of its area covered by the relevant catchment, where the. The catchment boundaries were obtained from readily available GRDC (Lehner, 2012) and GSIM (Do et al., 2018) databases., with GRDC being prioritized when the boundary of a catchment was available in both databases. Note that for smaller catchments under 100 km^2 (approximately 0.1° × 0.1°), uncertainties may exist due to the relatively coarser spatial resolution of the meteorological data. Nonetheless, those catchments with large uncertainties will not be considered for the subsequent attribution analysis if ML models cannot capture the relationship between inputs and outputs effectively. Day length was included in the study since it was shown to improve model accuracy in a series of preliminary tests. It, including the cases where only precipitation and temperature were used and day length was additionally incorporated. Catchments where day length largely improves accuracy are mainly located in northern Europe. Day length was calculated based on the day of the year and the latitude of the catchment center by the Brock model following Forsythe et al. (1995).
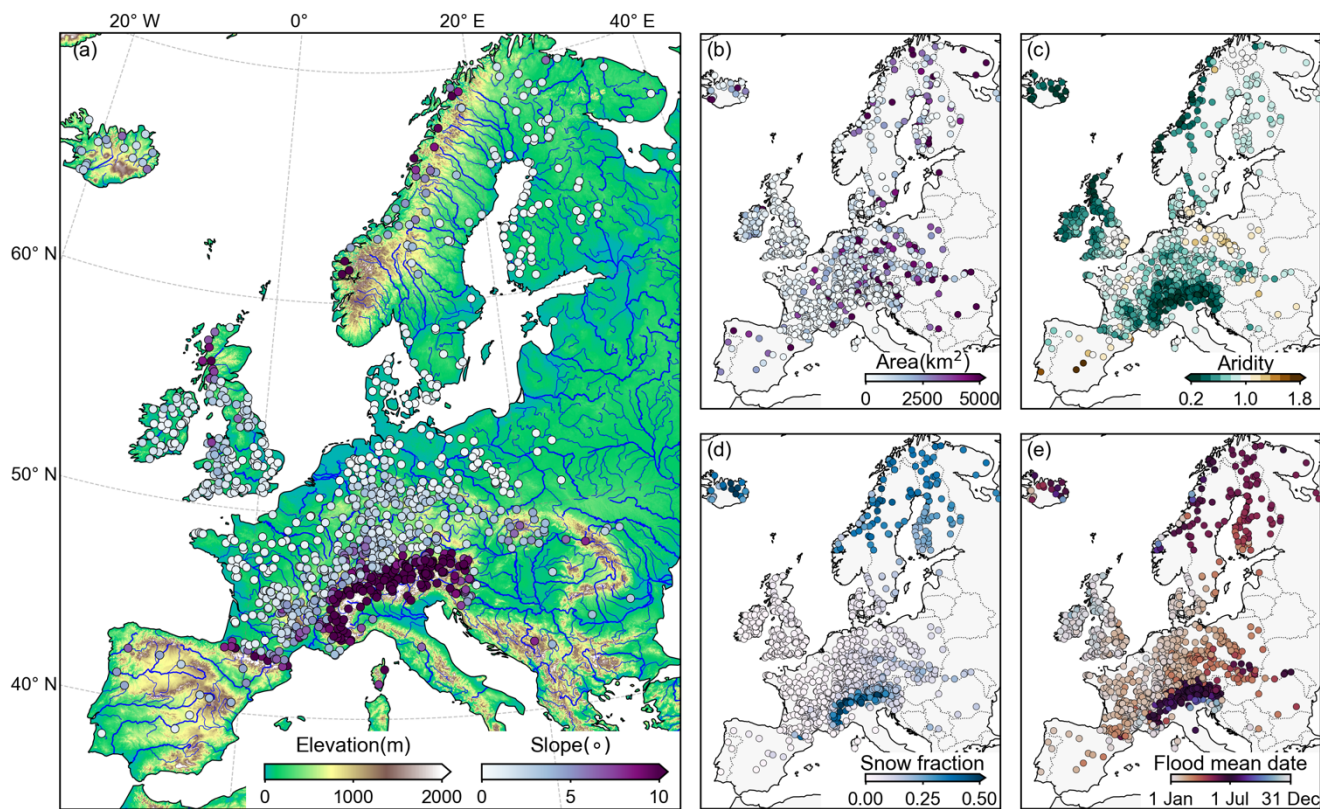
Figure 1: An overview of the 1,077 catchments and their properties, including average (a) elevation and slope of the catchments, (b) the catchment size, (c) the aridity index, expressed by the ratio between mean annual potential evapotranspiration (PET) over mean annual precipitation, (d) the fraction of precipitation falling as snowfall (i.e., precipitation falling with temperature below 0 °C), and (e) the seasonality of annual maximum discharges. PET was estimated via Hamon's formulation (Hamon, 1961).

2.2 Attribution framework and ML model

Figure 2 illustrates the framework of using explainable ML methods for flooding attribution in the present study, which was originally developed by Jiang et al. (2022) and involves three main steps. First, we built ML models for individual catchments to establish the nonlinear predictive maps from meteorological factors (i.e., precipitation, temperature, and day length) to daily discharges (Fig. 2a). Secondly, an ML interpretation technique was applied to interpret the trained models to quantify the contributions of the three input variables at each time step (i.e., time-wise feature importance) to the generation of respective flood events (Fig. 2b). The time-wise feature importance was further aggregated into contributions of specific features. Finally, cluster analysis was used to group the specific feature contributions from multiple flood events that had similar patterns into several categories, from which we then identified different flood mechanisms ~~(Fig. 2c)~~. Detailed explanations of the methods are given below.
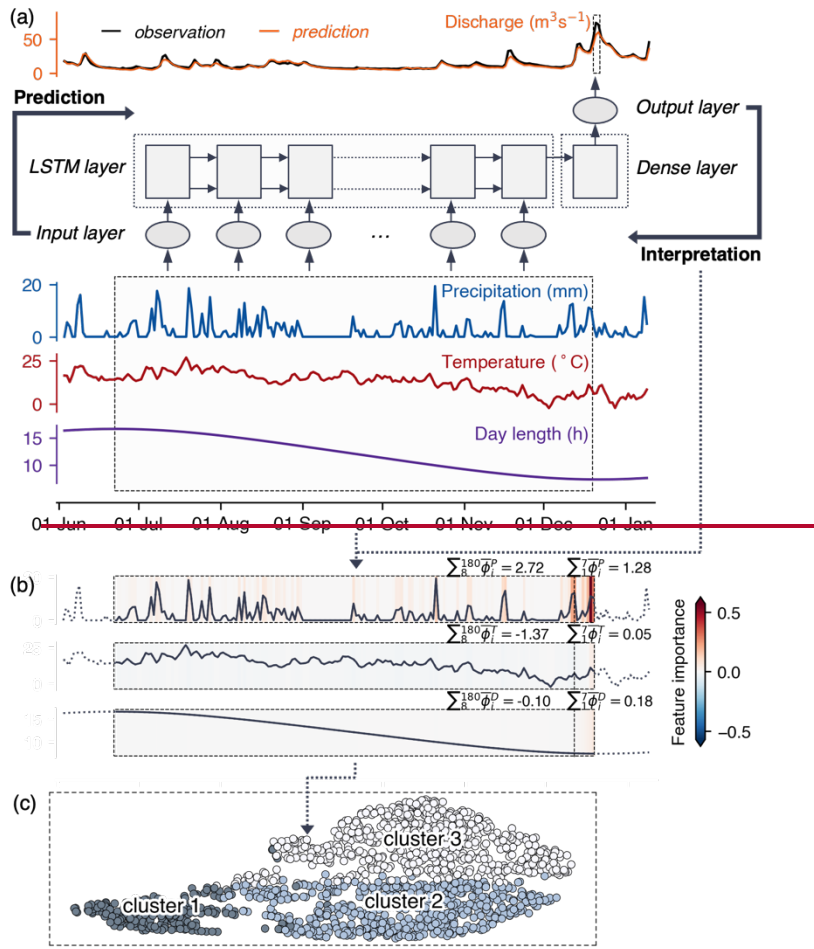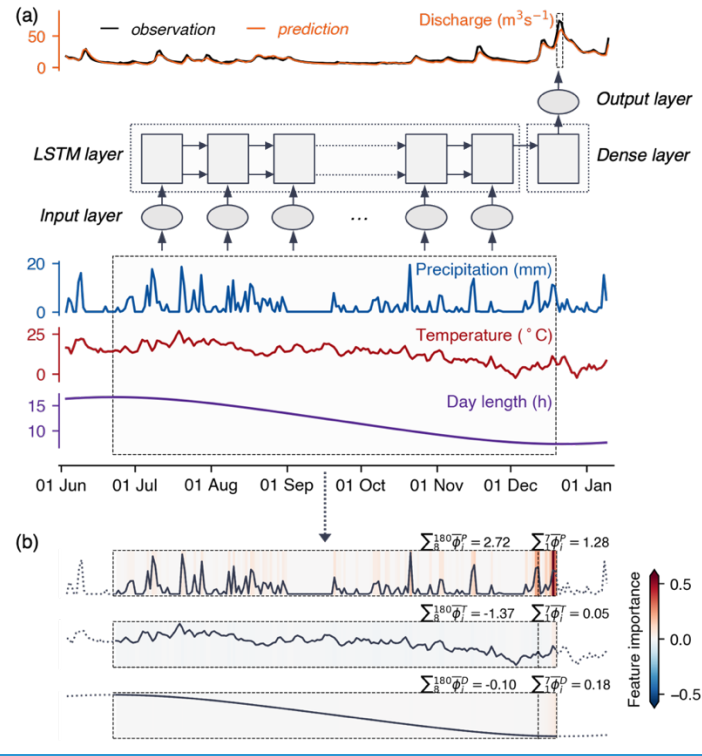
Figure 2: The workflow of using explainable ML methods for attributing flood peaks (annual maxima of river discharge) to their drivers. (a) Diagrammatic representation of the used LSTM models~~, where the windows~~. The window in the time series of discharge highlights the target output (which is a point) and the window in the inputs ~~and output highlight~~indicates the input features ~~and target output in predicting~~used to predict the illustrated peak discharge sample. (b) The feature importance ~~extracted~~of the inputs for predicting the peak discharge shown in (a), which was obtained by using the ML interpretation technique (namely integrated gradient ~~(IG) technique for the flood event shown in (a).~~). The vertical dashed lines in the windows separate the feature importance into a recent 7-day period and an earlier period to calculate the aggregated feature contributions (see main text). ~~(c) A subset of peak discharges visualized by using t-Distributed Stochastic Neighbor Embedding (t-SNE), where each dot represents one peak discharge event and the clusters are obtained based on the results.~~

In the study, we used the classical LSTM network (Hochreiter and Schmidhuber, 1997) as the ML model. The LSTM is one of the most popular ML architectures for modeling dynamic hydrological variables (e.g., Kratzert et al., 2018; Lees et al., 2021), which can effectively capture nonlinear and temporal dependencies between variables owing to its recurrent structure and unique gating mechanism (Gers et al., 1999). The effectiveness of the LSTM is partially due to the comparability of its formulation to the hydrological behavior of a catchment. Specifically, the backbone of the LSTM network is composed of recurrent cells that can store previous information from input sequences, which is conceptually similar to the way meteorological information (e.g., precipitation) is stored in the form of soil moisture or snowpack (Lees et al., 2022). The physically realistic mapping from inputs to outputs facilitates gaining hydrologically meaningful insights from subsequent model interpretations. Figure 2a illustrates the data flow of one sample in the LSTM model, with the dashed windows highlighting the predictors and the target variable. The input layer of the model brings in precipitation (P), temperature (T),

and day length (D) over the past 180 days (i.e., $[X_1^P, X_2^P,..., X_{180}^P; X_1^T, X_2^T,..., X_{180}^T; X_1^D, X_2^D,..., X_{180}^D]$) and the output layer produces the discharge of the following day (i.e., y_0). The hidden layers consist of a single LSTM layer and a dense layer with 32 units. The number of time steps and hidden units were determined by considering both the model performance and efficiency, which had been evaluated in preliminary experiments. Preliminary experiments also suggest using fewer time steps (e.g., 90 days) would not impair the ~~later~~ conclusions of the study about flooding mechanisms, because contributions from inputs at very early time steps to output are limited in LSTM models (i.e., memory decay) (Su and Kuo, 2019). Here, we skip the technical details of the LSTM architecture and refer to Sherstinsky (2020) for a comprehensive explanation of the fundamentals of LSTM networks.

~~Given a catchment,~~ To improve the robustness of model evaluation and analysis, we fitted 10 independent LSTM models for each of the 1,077 catchments. Each independent model was trained and tested based on samples that were randomly split in a 7-to-3 proportion~~, where the random sampling strategy enables capturing the overall hydrometeorological variability observed across various periods. In the training process,~~. During the training process, a portion of the training data (70%) was repeatedly used to update the model parameters every epoch until no further decrease in the loss function was observed on the remaining 30% (also known as validation data). The trained models were independently evaluated on the testing datasets. Note that here we adopted a random sampling strategy instead of the time-series splitting strategy with fixed time intervals in order to enable capturing the overall hydrometeorological variability observed across various periods. It should be emphasized that while the random sampling strategy is appropriate with respect to the purpose of this study, it might not be the best practice if the models were developed for prediction tasks, particularly if they were to be applied to new datasets. The initial learning rate and maximum training epoch number were configured to 0.01 and 200, respectively, with the adaptive moments estimation (Adam) algorithm (Kingma and Ba, 2015) ~~was adopted to optimize the parameters of neural networks. The initial learning rate and maximum training epoch number were configured to 0.01 and 200, with an early stopping strategy to prevent overfitting.~~ being used for training the models.

2.3 Model interpretations and cluster analysis

The integrated gradient (IG) technique developed by Sundararajan et al. (2017) was employed to interpret the trained models, which allows for obtaining the time-wise feature importance of the three input variables for each sample~~.~~ of the output (i.e., daily discharges). The IG method is a gradient-based interpretation technique that exploits the gradient of the model's output to its input features to trace back the specific contributions of the inputs. It aims to assign an importance score to each feature (e.g., to the precipitation at each time step prior to the flooding). A large positive score indicates that the feature substantially increases the network output (e.g., that the precipitation at a certain time step contributes to increasing the flooding), a large negative score indicates a decrease in the network output, and a score close to zero indicates little influence on the output. The IG score for the input feature x (e.g., precipitation at the i-th time step) is formulated as:

190
$$\phi_i(x) = (x_i - x_i') \int_{\alpha=0}^{1} \frac{\partial f(x' + \alpha(x-x'))}{\partial x_i} \, d\alpha \qquad (1)$$

where $\frac{\partial f(x' + \alpha(x-x'))}{\partial x_i}$ denotes the local gradient of the network f at a point interpolated from a baseline input (x', when $\alpha =$ 0), which is meant to represent the "absence" of feature input, to the target input (x, when $\alpha = 1$). An important property of the IG is completeness, which states that the IG scores add up to the difference between the output of f at the target input x and the baseline input x', i.e., $\sum_i \phi_i(x) = f(x) - f(x')$. Therefore, the model output can be decomposed into the sum of

195 features' individual contributions, and it enables us to examine the contribution of a group of features by summing up their individual IG scores.

In the study, we focus specifically on the IG scores for annual maximum peak discharge events to gain insights into flooding mechanisms. Given that we trained 10 independent models, 10 sequences of time-wise feature importance were generated for

200 each peak discharge, with each sequence having the same dimensions as the input variables (i.e., $[\phi_1^P, \phi_2^P, ..., \phi_{180}^P; \phi_1^T, \phi_2^T, ..., \phi_{180}^T; \phi_1^D, \phi_2^D, ..., \phi_{180}^D]$). Then, the 10 sequences were averaged into one sequence (i.e., $[\bar{\phi}_1^P, \bar{\phi}_2^P, ..., \bar{\phi}_{180}^P; \bar{\phi}_1^T, \bar{\phi}_2^T, ..., \bar{\phi}_{180}^T; \bar{\phi}_1^D, \bar{\phi}_2^D, ..., \bar{\phi}_{180}^D]$, which is simplified as $\{\bar{\phi}_i\}$ hereafter) to reduce the impact of the stochasticity associated with training the different LSTMs. Figure 2b exemplifies the averaged IG scores corresponding to the sample shown in Fig. 2a, i.e., it shows the contribution of the three input variables to the selected annual maxima of river discharge. The warm or cool colors in the

205 heatmap denoting the input variable at the particular time step has increased or decreased the network output, while white indicates little effect. Note that the averaged IG scores for an individual peak were computed by averaging the scores obtained from all the independent 10 models, regardless of whether the peak was part of the training data or the testing data in the models. Overall, the IG scores extracted from the 10 models for each target peak discharge generally follow a similar pattern, though with inevitable differences due to randomness and uncertainties in training processes (see Figs. S1–S3 in the

210 Supplementary Material for examples).

In the following step, the sequences of averaged IG scores $\{\bar{\phi}_i\}$ can be clustered directly using time series clustering techniques based on their similar shapes, such as using the K-means method with the dynamic time warping algorithm (DTW) as the distance metric (Tavenard et al., 2020). However, the main drawback of clustering time series is the heavy computational

215 burden. The DTW distance between any two samples has a quadratic time complexity with respect to the sequence length, which would make clustering long feature importance sequences a time-consuming process, and it would be especially challenging when dealing with tens of thousands of sequences (Salvador and Chan, 2007). Moreover, for this large-sample study that aims to understand flood mechanisms at a continental scale, it might not be necessary to distinguish the daily contributions of meteorological drivers in detail. Therefore, before carrying out the cluster analysis, we aggregated each

220 sequence of averaged IG scores $\{\bar{\phi}_i\}$ ~~into~~by using a 7-day separating window, which generate a low-dimensional contribution vector with only six elements $[\sum_1^7 \bar{\phi}_i^P, \sum_8^{180} \bar{\phi}_i^P, \sum_1^7 \bar{\phi}_i^T, \sum_8^{180} \bar{\phi}_i^T, \sum_1^7 \bar{\phi}_i^D, \sum_8^{180} \bar{\phi}_i^D$ ~~], where~~]. Here $\sum_1^7 \bar{\phi}_i$ and $\sum_8^{180} \bar{\phi}_i$ represent

contributions of a variable in recent 7 days and an earlier antecedent period, respectively. The separating window size should cover the period of precipitation and snowmelt events leading to each peak discharge, which depends highly on the local characteristics. After examining the relationship between catchment area and mean event response time, Stein et al. (2020)The selection of 7 days accounts for the entire flood-generation and routing processes for catchments investigated in the study, and is also consistent with the majority of suggested a synoptic window of 7 days should be sufficient to guarantee the response time for large catchments. As a result, this study used a 7-day period, similar to the practice in most studies that examined flooding causes (e.g., Blöschl et al., 2017; Berghuijs et al., 2019). However, using a shorter period (e.g., 5 days) does not affect the conclusions about dominant flooding mechanisms and their trends (see discussion in Section 3.7). Figure 2b demonstrates the values of the aggregated feature contributions based on respective daily IG scores represented by the heatmap.

To obtain an overall picture from the individual aggregated feature contributions, we used the K-means method to cluster the results for multipleall annual maximum peak discharges pooled from all considered catchments, we used the K-means method to cluster aggregated feature contributions into groups with similar patterns (as illustrated in Fig. 2c). Considering that the feature importance values are correlated to the magnitude of the predicted peak discharge due to the completeness property, we normalized each accumulated vector by its Manhattan norm (i.e., dividing each element by the sum of its absolute values while keeping its sign) to make the contributions comparable across different floods. To determine the optimal cluster number for the K-means algorithm, we evaluated the cluster characteristics for candidate cluster numbers ranging from 2 to 8 using the silhouette coefficient (Rousseeuw, 1987), which reflects the separation distance between the resulting clusters. The silhouette coefficient for an individual sample is calculated as $(b - a)/\max(b - a)$, where a represents the mean distance between the sample to all other points within the same cluster, and b represents the mean distance between the sample and all other points in the next nearest cluster. The average silhouette coefficient over all samples is an indicator of the goodness of a clustering result, which ranges from -1 to 1, with a higher score generally indicating a better cluster number choice.

2.4 Trend analysis of flooding mechanisms

Based on the clustering results, we can identify the mechanism responsible for each annual maximum peak discharge and calculate the proportions of different flooding mechanisms at either the continental or catchment scale. The trend magnitude in these proportions was then analyzed by the Theil-Sen's Estimator, with the modified Mann-Kendall test (Hamed and Rao, 1998) being used to determine the significance of the trend. Specifically, at the continental scale, we estimated the overall trends of various flooding mechanisms based on their respective proportions within all the annual maximum peak discharges per year. At the catchment scale, to capture the variations of flooding mechanisms over different periods, we calculated the proportion series using a 20-year moving window in each catchment. The 20-year time frame was used to ensure an adequate sample size for reliably estimating the intra-period proportions and also to guarantee enough periods to observe decadal variability (Pagano and Garen, 2005). Only proportions that were calculated with at least 10 years of peak discharge data in each window were used to estimate the trend slope.

Moreover, in order to analyze the possible causes of trends, we selected some catchments exhibiting significant changes in flooding mechanisms and compared the temporal regional changes in flooding mechanisms with changes in potential flooding drivers. The time series of proportions in regions were calculated by applying the previously described 20-year moving window to peak discharge classifications for the considered catchments. The flooding drivers considered include annual maximum 7-day total precipitation, mean spring temperatures (January to April), and 30-day precipitation preceding the 7-day window of recent precipitation, which is a common proxy for soil moisture prior to flooding (e.g., Bertola et al., 2021). All the drivers were averaged across the catchments and then smoothed by using a 20-year moving average window as well.

3 Results and ~~discussions~~discussion

3.1 Model predictive performance and interpretations

Before moving to the analysis of annual maximum peak discharges, we used the Nash-Sutcliffe efficiency (NSE) (Nash and Sutcliffe, 1970) to assess model accuracy in predicting discharges. The NSE value ranges from negative infinite to 1.0, and NSE > 0.5 is generally deemed satisfactory for discharge simulations (Moriasi et al., 2015). Based on the NSE value computed in the testing period for each independent model, we acquired the average and standard deviation of NSE values for each of the 1,077 catchments, as shown in ~~Figure~~Fig. 3. The overall warm colors in the map (Fig. 3a) indicate that the model performed satisfactorily for most catchments, with the median of NSE averages reaching 0.81 (Fig. 3b). The low standard deviations of NSE values (Fig. 3c) further indicate robust model performance in most cases. Accordingly, the models have effectively captured the generalizable predictive relationship between meteorological factors and discharges. As an accurate and robust predictive relation is essential for deriving meaningful information from ML models (Murdoch et al., 2019), the subsequent analyses focus specifically on the 1,009 catchments (out of 1,077; 94%) with average NSE values above 0.5 and coefficients of variation below 0.1. In the following, we move to the analysis of annual maximum peak discharges.
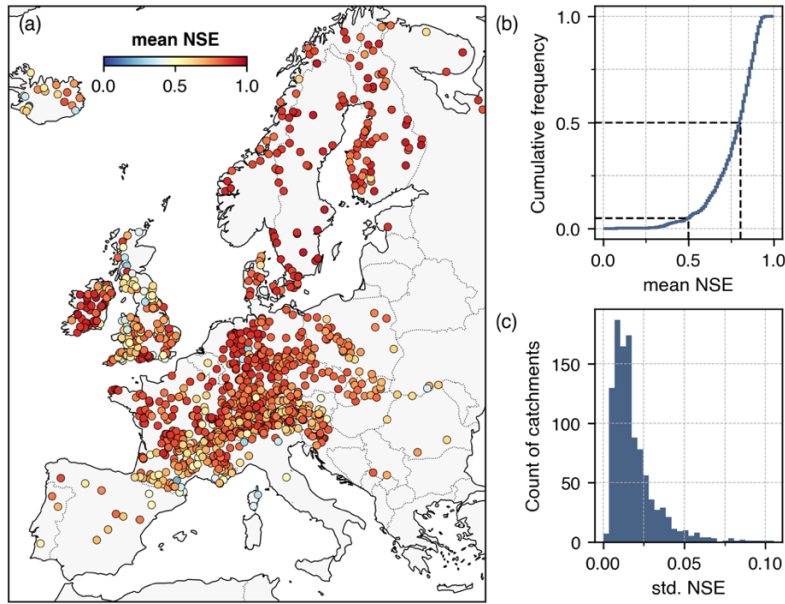
Figure 3: (a) Nash-Sutcliffe efficiency (NSE) values in the evaluation period averaged over the 10 independent LSTM models. (b) The cumulative frequency of the averaged NSE values. (c) The distribution of the standard deviation values for the NSE values across the 10 independent models. The NSE values were calculated using all samples in respective testing datasets.

A total of 55,828 annual maximum discharges were identified from the 1,009 catchments (20–70 peaks per catchment). By using the IG method, we can obtain 55,828 feature importance sequences averaged across the 10 independent models. In the case shown in Fig. 2c2b, precipitation is the dominant driver behind the annual maximum peak discharge occurrence, showing consistently non-negative feature importance with the precipitation peaks that occur closer to the target flood peak having a greater influence (see pronounced positive contributions in red). Nevertheless, the total contribution from antecedent precipitation is more important in predicting the peak compared with the contribution from recent precipitation, as indicated by the aggregated scores $\sum_1^7 \bar{\phi}_i^P$ and $\sum_8^{180} \bar{\phi}_i^P$. The temperature, on the other hand, has an overall negative impact, which may be related to evapotranspiration that could decrease the discharge magnitude, while the influence of the day length is relatively negligible. Additionally, Fig. 4 further illustrates two other typical cases of feature importance patterns, where the contribution from recent precipitation (i.e., $\sum_1^7 \bar{\phi}_i^P$) and temperature (i.e., $\sum_1^7 \bar{\phi}_i^T$), respectively, is dominant in predicting target peak discharges. The distinct patterns of predictor contribution to annual maximum peak discharge predictions suggest that these flood events were triggered by different mechanisms.
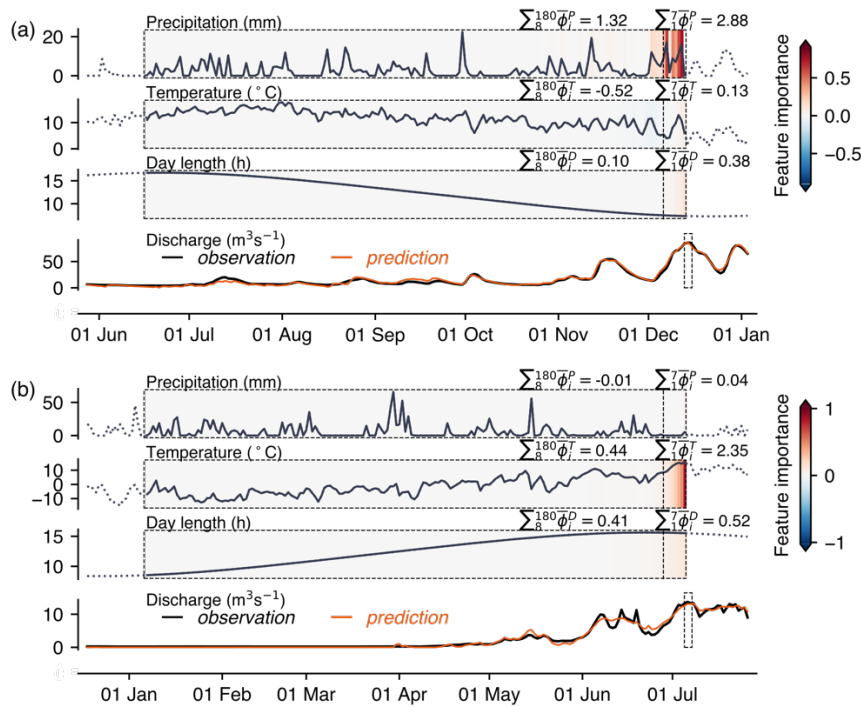
Figure 4: Additional examples to the case shown in Fig. 2, which illustrate the importance pattern of temperature, precipitation, and day length in predicting two discharge peaks from other catchments. (a) Recent precipitation contributes most to the discharge peak. (b) Recent temperature contributes most strongly to the discharge peak.

3.2 Flooding types revealed by cluster analysis

To separate the 55,828 annual maximum peak discharges into discrete groups characterized by distinct patterns of predictor contributions, we performed K-means clustering on the normalized contribution vectors. The results of the silhouette analysis suggest that clustering into three main groups would lead to the best clustering quality, because it achieves the highest average silhouette coefficient and silhouette coefficients for individual samples are reasonably distributed within each cluster (see Fig. A1 in Appendix A for more details). It should be noted that the clustering results here only reveal major patterns widespread in data, with certain local and specific mechanisms unlikely to be detected.

Figures 5a–c show the distinct patterns of the three identified clusters, with cluster 1 featuring high importance of recent temperature (Fig. 5a, a positive contribution in line with high temperature favoring snowmelt), cluster 2 featuring the dominant contributions from recent precipitation (Fig. 5b), and cluster 3 featuring the importance of antecedent precipitation events (Fig. 5c). Compared to cluster 1, clusters 2 and 3 show a generally negative effect of antecedent temperature, in line with drying favored by evapotranspiration. Moreover, annual maximum peak discharges in cluster 1 are characterized by higher contributions from day length (Fig. 5a) when compared to the other two clusters. The role of day length implies that the magnitude of these peak discharges can be partially explained by the seasonality presented by day length, which peaks around

the June solstice. In contrast, the main differences between clusters 2 and 3 are due to the fractions of $\sum_1^7 \bar{\phi}_i^P$ and $\sum_8^{180} \bar{\phi}_i^P$.

Overall, each cluster accounts for 15.2%, 48.3%, and 36.5% of all the identified annual maximum peak discharges, respectively.
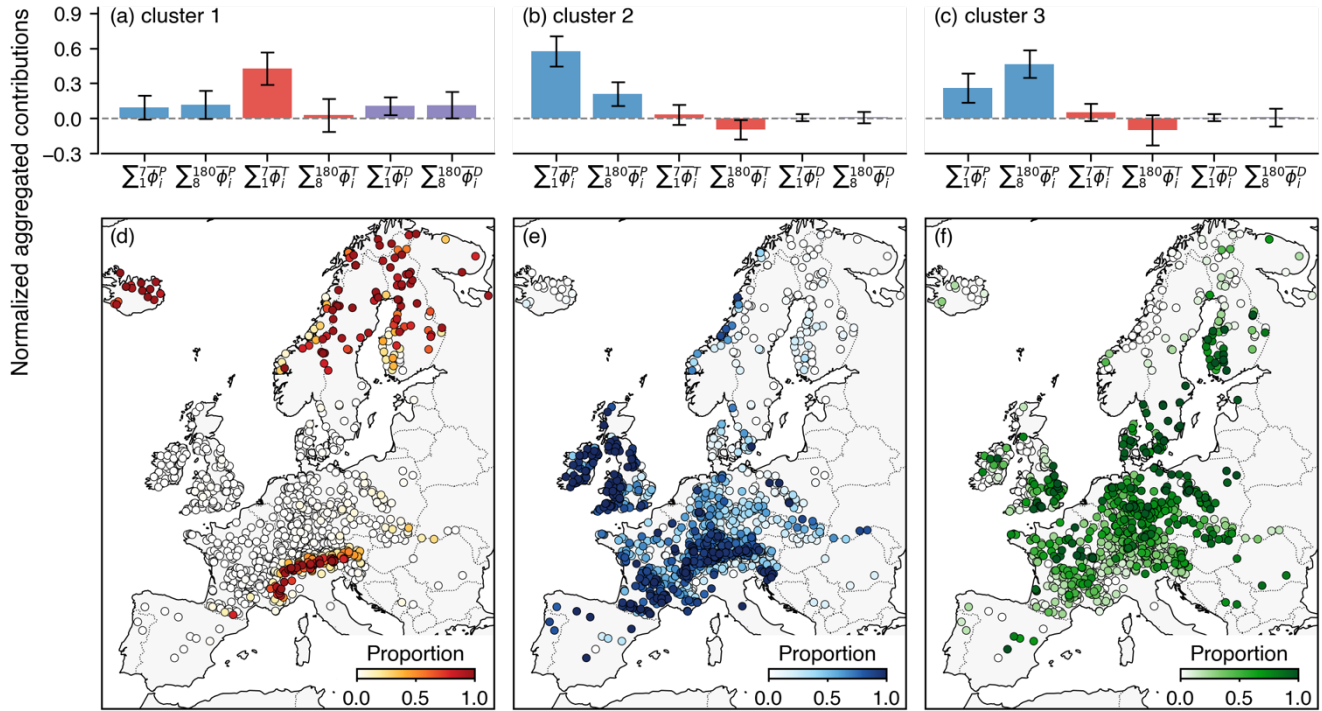
Figure 5: The cluster centroids and variance for the three clusters and their respective proportions of all peak discharge events in each catchment. The bars and error bars in (a), (b), and (c) represent the cluster centroids and standard deviations of the six aggregated feature contributions. The proportions in (d), (e), and (f) correspond to clusters 1–3, respectively.

Figures 5d–f illustrate the distributions in terms of the proportion of annual maximum peak discharges associated with each cluster within a catchment. Annual maximum peak discharges associated with high contributions from temperature (cluster 1) mainly occur in northern Europe and in mountainous regions such as the Alps (Fig. 5d), i.e., in ~~snowy~~ regions with high snowfall fractions (Fig. ~~1c~~1d) where rising air temperature can lead to snowmelt. The spatial distribution together with the feature pattern shown in Fig. 5a indicates that these floods were probably driven by snowmelt events. In contrast, catchments with cluster 2, where recent precipitation played a decisive role in causing most floods (Fig. 5b), are primarily located in regions that have a west-facing or north-west-facing coast or mountain range, such as Ireland, Scotland, Wales, the Norwegian coast, north-west of the Iberian Peninsula, as well as the area extending from the Alps, the Massif Central and the Pyrenees (Figs. 5e and 1a). These regions are characterized by a generally humid climate (Schiemann et al., 2018), as also indicated by Fig. 1c, and are strongly affected by the Northern Atlantic polar front and the associated storm tracks (Bengtsson et al., 2006) and/or by the presence of mountain barriers perpendicular to the prevailing flow direction, which force moist air to lift and

condense (Isotta et al., 2014). Previous studies indicate that flooding in the regions could be largely explained by individual heavy precipitation events (Gobiet et al., 2014; Blanchet and Creutin, 2017; Whan et al., 2020), some of which are associated

335 with atmospheric rivers (Lavers and Villarini, 2013).

Catchments ~~involved~~associated with cluster 3 are mostly located over the North European Plain, South Scandinavia, and parts of the British Isles (Fig. 5f). Here, information from antecedent precipitation has an overall higher weight than that from recent precipitation or other predictors (Fig. 5c), suggesting that recent precipitation alone would not suffice to explain annual

340 maximum peak discharges. Therefore, flooding in these areas presents additionally heavy reliance on antecedent precipitation that is stored in the form of soil moisture. For example, Nied et al. (2014) revealed that in the Elbe River basin some weather patterns only cause flooding in case of preceding soil saturation. Also, Ledingham et al. (2019) found that in southeast England fewer than 15% of daily flood events correspond to extreme precipitation events, lower than in the rest of Britain, which was attributed to the relevant contribution of soil moisture storage to flooding.

345

It should be noted that the three kinds of flooding mechanisms (i.e., snowmelt-driven, recent precipitation-driven, and antecedent precipitation-driven) identified from the cluster analysis using the optimal cluster number only indicate which features carry greater weights for peak discharge predictions, and they are not necessarily mutually exclusive. Particularly, the peak discharge events near the decision boundaries between the three clusters, such as those with similar Euclidean distances

350 to at least two different "closest" centroids, are likely affected by two or more flooding processes simultaneously. For example, the events categorized as snowmelt-driven floods are probably impacted additionally by saturated soils or extreme precipitation, such as rain-on-snow events (Cohen et al., 2015). ~~Likewise, soil can be saturated before recent precipitation-driven floods, and flooding primarily driven by excessive soil moisture can be exacerbated by heavy rain .~~ These events generally represent compound flood events that arise from several drivers occurring concurrently (Zscheischler et al., 2018; Bevacqua et al., 2021).

355 Recently, compound events have received increasing attention (Zscheischler et al., 2020), however, this study will only focus on the main flooding types obtained from the clustering results, regardless of whether compound effects were involved.

3.3 Dominant flooding mechanisms in Europe

The result of event-based flooding classification allows us to identify the dominant flooding mechanisms (among clusters 1–3, Fig. 5) for each catchment (Fig. 6a). A mechanism is considered dominant in a catchment if the proportion of the annual

360 maximum peak discharges exceeded the maximum proportion of the other annual maximum peak discharges by more than 70%. Otherwise, the catchment was regarded as being dominated by a ~~mix~~mixture of flooding mechanisms. The ~~mixed~~mixture of mechanisms could be further classified into specific combinations based on which clusters were present in the catchment. Accordingly, for the catchments investigated in the study, 52.8% were dominated by ~~mixed~~a mixture of mechanisms, while snowmelt, recent precipitation, and antecedent precipitation solely accounted for 25.6%, 12.3%, and 9.3% of catchments,

365 respectively. Among the ~~mixed~~mixtures of mechanisms, the combination of recent precipitation and antecedent precipitation

accounted for 33.2% of all the catchments, followed by the combination of all three mechanisms (16.5%), the combination of recent precipitation and snowmelt (1.9%), and the combination of antecedent precipitation and snowmelt (1.2%).
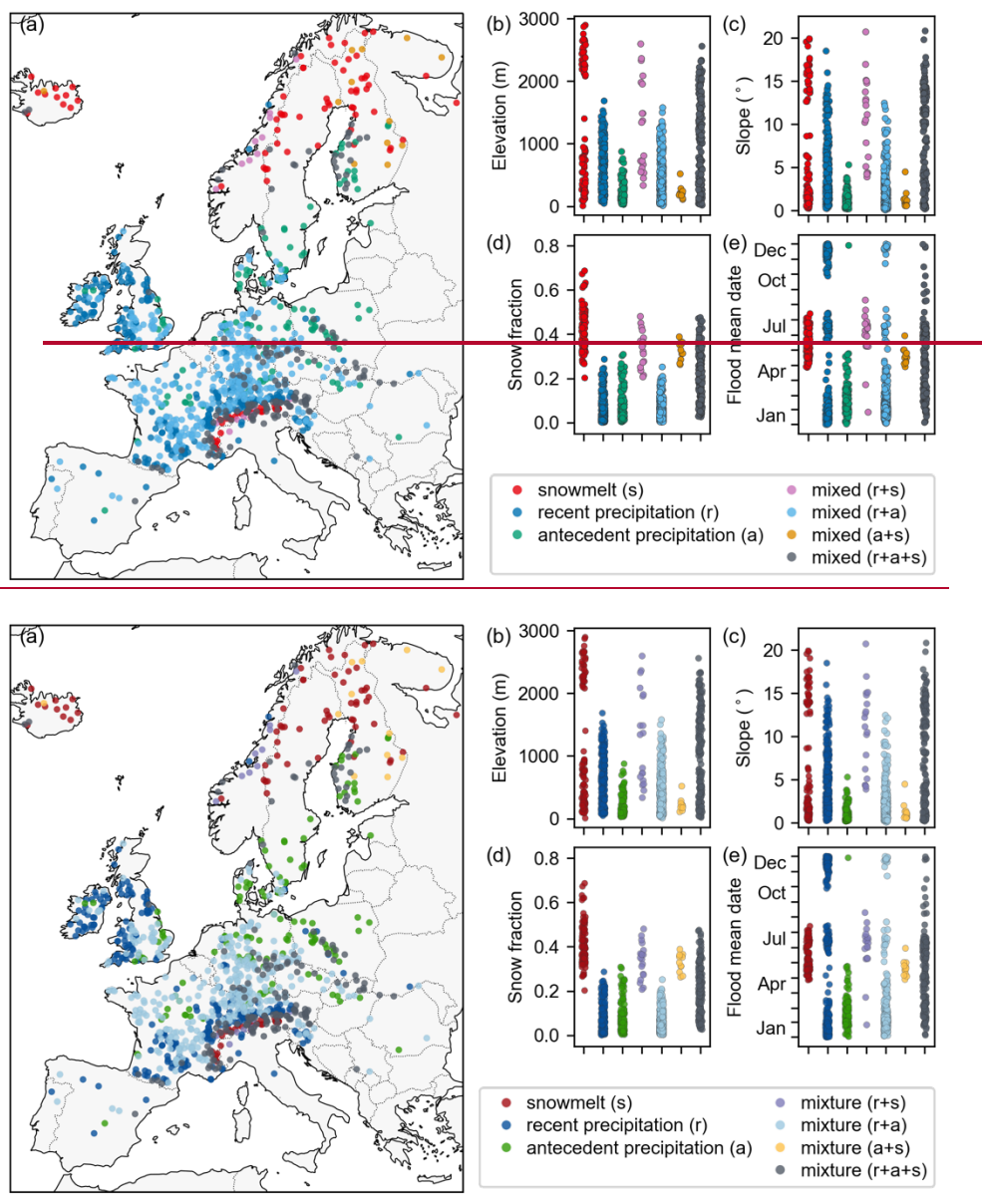
Figure 6: The dominant flooding mechanisms and their relevance to catchment attributes and seasonality. Each dot in (b), (c), (d), and (e) represents one catchment. Mixture means the associated catchments are dominated by two or more flooding mechanisms. For example, mixture (r+s) indicates either recent precipitation (r) or snowmelt (s) is the primary cause of the annual maximum discharges for the associated catchments, and the difference between the two proportions is less than 70%.

It is worth noting again that the presence of ~~mixed~~a mixture of flooding mechanisms in a catchment only indicates that annual maximum discharges in the catchment are not uniformly caused by the same mechanism, rather than signifying whether individual annual maximum peak discharge events are driven by multiple processes (i.e., compound events). Despite this, floods in catchments with ~~mixed~~a mixture of flooding mechanisms, in general, are more likely to be affected by two or more

380 flooding processes, since the classification of floods in these catchments can be ambiguous (e.g., the events near the decision boundaries between clusters). For example, floods caused by both heavy precipitation and excessive soil moisture tend to present high reliance on both recent precipitation and antecedent precipitation, which results in the catchment presenting ~~mixed~~a mixture of flooding mechanisms, depending on which feature importance is superior. Using 0.10 as a distance threshold to define events near the cluster decision boundaries (i.e., the difference between the distance from one point to its

385 closest centroids and to its second-closest centroids is less than 0.10), 77.1% of such events were found in catchments dominated by ~~mixed~~a mixture of mechanisms, whereas only 22.9% were found in catchments dominated by single mechanisms.

In Figs. 6b–e, we further examine the relevance of dominant mechanisms to catchment physiographic and hydroclimatic characteristics demonstrated in Fig. 1. Unsurprisingly, snowmelt dominates flooding in regions with high snowfall fractions

390 and obvious characteristics in latitude and altitude, where floods usually occur from May to July. The catchments dominated by antecedent precipitation are within plain terrains, where flooding occurs mainly during the winter and spring. Catchments with a gentle slope generally tend to have thicker soil, slower transmission, and therefore more potential to store antecedent precipitation (Hallema et al., 2016). In contrast, recent precipitation-dominated catchments have a broader spectrum of slopes and elevations and experience also summer floods. The distribution of catchment attributes from catchments dominated by

395 ~~mixed~~a mixture of mechanisms ~~are~~is consistent with what we found based on catchments dominated by a single mechanism. For example, catchments dominated by snowmelt mixed with recent precipitation (~~pink~~purple in Fig. 6) or antecedent precipitation (~~orange~~yellow in Fig. 6) have relatively high snowfall fractions, with the former mainly occurring on areas with steep slopes (mainly in the Alps and Scandinavian mountains) and the latter mainly occurring on gentle slopes (such as parts of Finland). The catchments controlled by both recent and antecedent precipitation (light blue in Fig. 6) are located mostly in

400 western Europe, suggesting that floods there were likely to be affected by the interaction between extreme precipitation and antecedent soil moisture, and their respective relative importance has varied between events. In addition, some catchments in the Alps, Germany, and Poland are impacted by all three mechanisms (slate grey in Fig. 6). In summary, these findings indicate that dominant flooding mechanisms differ substantially across catchments and are related to their geographic and climatic characteristics. In addition to elevation, slope, and snow fraction, the study by Stein et al. (2021) on catchments in the United

405 States demonstrated that other catchment characteristics (e.g., aridity, precipitation seasonality, and mean precipitation) also significantly influence flood generating processes. An in-depth investigation of how geographic and climatic characteristics affect flood mechanisms in European catchments can be expected in future studies.

3.34 Comparative analysis with other studies

A better understanding of the generating processes of river flooding is crucial for interpreting past flood changes and improving future flood-risk predictions. In recent years, large-scale quantitative investigations of flooding mechanisms specifically for Europe have been undertaken in several studies, with different methodologies and scales applied. For example, by using circular statistics analysis, Berghuijs et al. (2019) examined the relative importance of three flooding mechanisms based on the seasonality of floods and three potential drivers such as the largest daily precipitation, the largest daily soil moisture excess, and the largest daily snowmelt. Bertola et al. (2021) attributed changes in the magnitude of flood quantiles to changes in possible drivers by using regression analysis and determined their contributions to flood changes accordingly. In contrast to these analyses conducted at catchment or coarser levels, Kemter et al. (2020) and Stein et al. (2020) performed event-based classifications to determine flooding mechanisms in respective regions or catchments, both using ~~manual~~predefined criteria but with different indicators and thresholds. Table 1 summarizes the main findings in these studies regarding the major flooding mechanisms per geographic subregion of Europe and compares them with those identified in this study.

Table 1. Comparisons of identified flooding mechanisms in Europe by different methods.

	Methods used	Research scales	Catchment sizes (km²)	Northern Europe	Western Europe	Central Europe	Southern Europe	Alpine
This study	Machine learning	Event-based	8 – 10,000	Snowmelt	Antecedent precipitation+ recent precipitation	Antecedent precipitation+ recent precipitation, snowmelt	*Lack of samples*	Recent precipitation, snowmelt
Berghuijs et al. (2019)	Seasonality analysis	Catchment-based	~10 – ~100,000	Snowmelt	Soil moisture	Soil moisture, snowmelt	Soil moisture	Extreme precipitation, snowmelt
Bertola et al. (2021)	Changes attribution	200 km × 200 km	5 – 100,000	Snowmelt	Extreme precipitation	Extreme precipitation, snowmelt	Soil moisture	Extreme precipitation, snowmelt
Kemter et al. (2020)	Multi-criteria	Event-based	1 – 800,000	Snowmelt	Soil moisture	Rain-on-snow, soil moisture	Soil moisture	Stratiform rainfall
Stein et al. (2020)	Multi-criteria	Event-based	1 – ~2,000,000[*]	Snowmelt	Excess rainfall	Snow/rain, Excess rainfall	Excess rainfall	Short rainfall

Note: The summaries above were compiled from relevant figures or qualitative descriptions in the respective studies, and the subregions of Europe were not strictly defined. The definitions of various flooding mechanisms were not identical between the studies. [*] The catchment size range was not stated in the paper, and we calculated it from the original results provided by the authors.

As indicated in Table 1, despite the different definitions, methods, and standards in recognizing flooding mechanisms, the five studies present some consistency, especially in Northern Europe and the Alps, which are dominated by snowmelt or by snowmelt combined with extreme precipitation. Among the four previous studies, this study shows the largest consistency with Berghuijs et al. (2019), especially when it comes to the contribution of meteorological drivers to flood generation in individual catchments. However, Berghuijs et al. (2019) and Kemter et al. (2020) regarded floods in regions from northern France to northern Germany as a consequence of soil moisture excess almost exclusively. In contrast, Bertola et al. (2021) and this study included extreme precipitation also as a crucial factor, and we have demonstrated that floods in those regions are driven by a combination of both heavy precipitation and saturated soil moisture. ~~Compared to analyses at catchment or coarser levels, event-based investigations of flooding mechanisms have the advantage of allowing for the detection of stronger signals about their potential changes over time, since averaged information tends to obscure information about individual event processes and thus makes the trends imperceptible. For example, found no discernible change in the relative importance of flood drivers for most regions in Europe, while some regional studies have indicated such changes .~~

In addition to methodological differences, ~~discrepancies in the estimation of soil moisture might~~ the inconsistent catchment samples are also ~~contribute to~~responsible for the divergent attribution results in different studies. As shown in Table 1, the catchments examined in this study are generally smaller, which tend to be more susceptible to rainfall with high intensity. Moreover, discrepancies in the estimation of soil moisture might be an additional reason. In the absence of direct observations, soil moisture in the four previous studies was explicitly estimated by using simple water balance models (Berghuijs et al., 2019; Stein et al., 2020), reanalysis data (Kemter et al., 2020), and a proxy based on antecedent precipitation (Bertola et al., 2021). The uncertainty associated with soil moisture estimates may, however, make a difference in determining whether floods are triggered by extreme precipitation or soil moisture excess. Tarasova et al. (2020)~~In contrast~~ conducted a rigorous uncertainty analysis of input data for a runoff event classification framework, emphasizing the importance of developing novel indicators to reduce these uncertainties. Here, profiting from the memory property of LSTM models, the present study identified flooding mechanisms based on long-term predictive relationships between precipitation, temperature, day length and discharge. The method has reduced the need for accurate catchment wetness estimates, yet such uncertainty is not eliminated completely, particularly since we chose a 7-day window to separate between antecedent and recent precipitation. Compared to analyses at catchment or coarser levels, event-based investigations of flooding mechanisms have the advantage of allowing for the detection of stronger signals about their potential changes over time, since averaged information tends to obscure information about individual event processes and thus makes the trends imperceptible. For example, Berghuijs et al. (2019) found no discernible change in the relative importance of flood drivers for most regions in Europe, while some regional studies (e.g., Beniston and Stoffel, 2016; Vormoor et al., 2016) and event-based studies (e.g., Kemter et al., 2020) have indicated such changes.

3.45 Temporal evolutions of flooding mechanisms

To test whether the dominant mechanism has changed over the period 1950–2020, we first compared the catchment-level dominant mechanisms separately for 1950–1985 and 1985–2020 by applying the procedure ~~described~~implemented in Section 3.~~2~~3. Only the 846 catchments with at least 15 years of records in each period were considered. Figure 7a summarizes the proportions of the single dominant mechanisms (represented by colorful blocks) and their combinations (represented by grey blocks) during each period along with shifts between them. The Sankey plot indicates that a majority of catchments (81.9%) retain their dominant mechanisms, and there has not been a shift from one dominant mechanism to another (see the absence of data flow between two different blocks from left to right). However, some catchments with single mechanisms have become dominated by ~~mixed~~a mixture of mechanisms (i.e., flowing from colorful blocks to grey ones, which accounts for 6.4% of the total), while some behave in the opposite way (7.4%). In a few catchments with ~~mixed~~a mixture of mechanisms (4.3%), the dominant mechanisms have also changed, though they remain mixed.

Despite only a few fractions of catchments presenting a change in their dominant flooding mechanisms, Fig. 7b reveals tendencies for specific mechanisms at event levels ~~as shown~~when considering all annual maximum peak discharges in the 846 catchments over the past seven decades. ~~The colorful lines represent~~In particular, the annual ~~evolution of the proportions of peak discharges that are associated with different flooding mechanisms, with the shades denoting the 95% confidence interval of the proportions. The magnitude of the monotonic trend was estimated by the Theil-Sen's Estimator as illustrated by the dashed lines, with the modified Mann-Kendall test being used to determine the significance of the trend. The~~maximum peak discharges driven by snowmelt have been declining by 0.7% per decade, while recent precipitation has become more dominant in causing floods, increasing by 1.0% per decade. Both frequency changes are probably associated with the warming atmosphere, which causes decreased snowpack (Fontrodona-Bach et al., 2018). Also, because of the rising temperatures, the atmosphere has a higher moisture holding capacity, leading to an increase in precipitation extremes on average (Trenberth, 2011; Fischer and Knutti, 2016). These factors make it more likely that the annual floods are driven by recent precipitation and less frequently by snowmelt. Additionally, we observe an overall slight decrease in soil moisture excess-driven floods as a result of counterbalancing the other two trends, though the trend is not statistically significant when considering the entire period. ~~Note that~~The above ~~conclusion is not affected even~~conclusions hold when considering a smaller subset of catchments (481 in the case) with at least 25 years of records in each period.
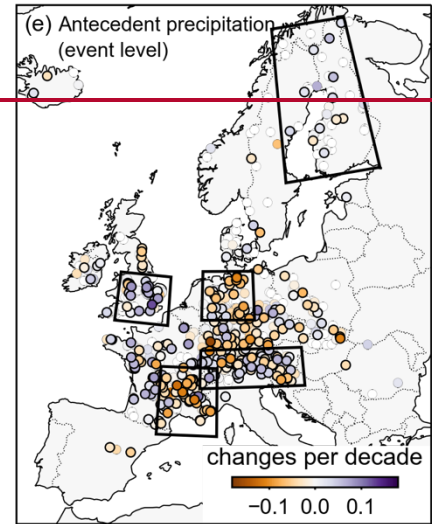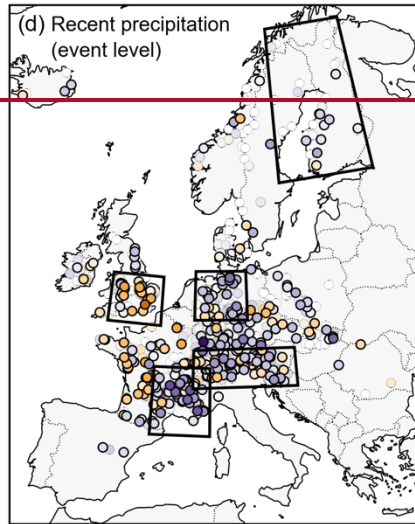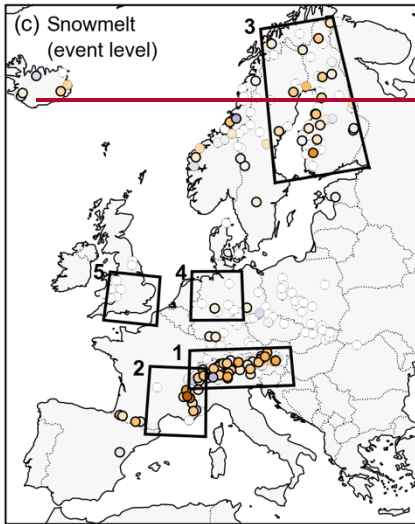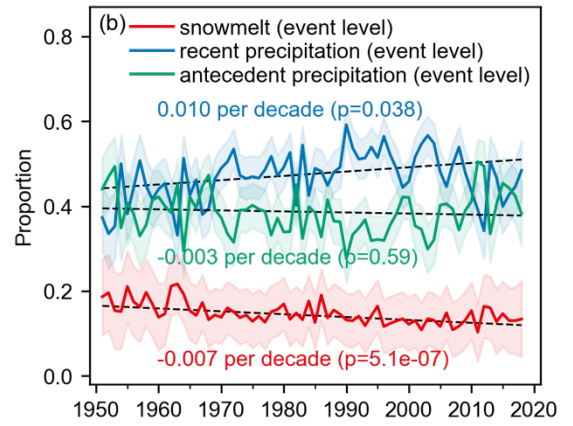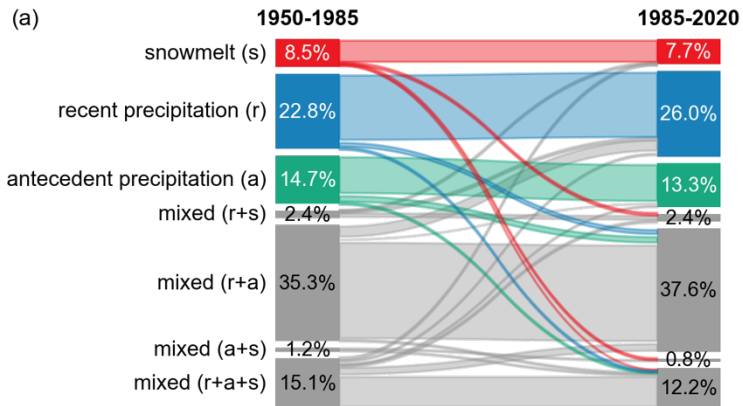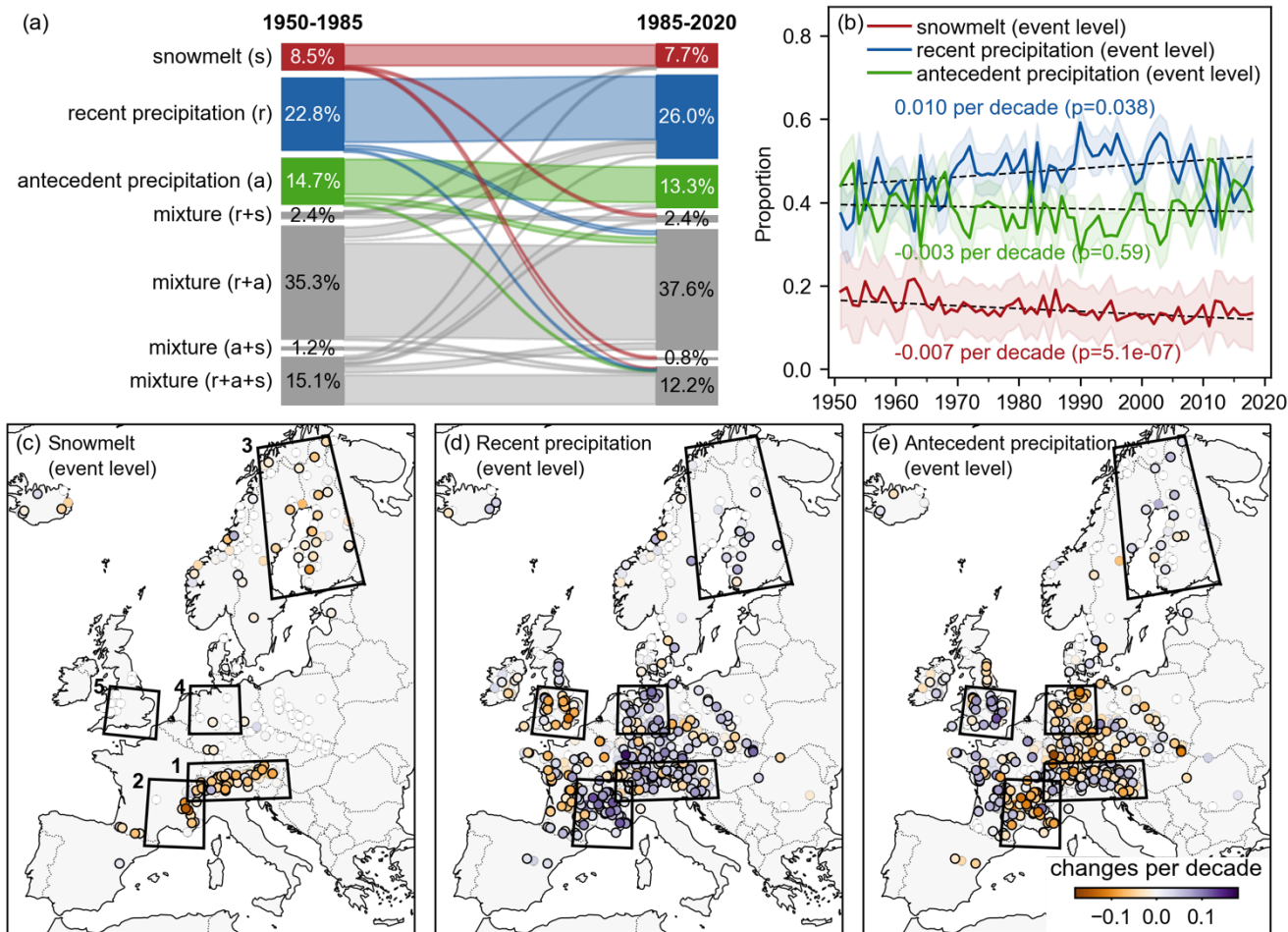
Figure 7: (a) Sankey plot indicating the proportions of single dominant flood generating mechanisms and their combinations during two time periods, with the flow lines indicating shifts between them. The proportions were calculated based on the 846 catchments that have at least 15 years of records available in each period. **(b)** The evolution of the proportions of annual maximum peak discharges with the three flooding mechanisms, with the shades denoting the 95% confidence interval of the proportions. The dashed black lines indicate the slope of their trends estimated by Theil-Sen's Estimator, with their significance being assessed by the modified Mann-Kendall test. **(c), (d), and (e)** The spatial trends in different event-based flooding mechanisms, where the trends indicated by the colorful dots were calculated using a 20-year moving window. Markers with black edges denote catchments with significant trends (α=0.05). The black boxes highlighted five hotspot regions that are discussed in the main text.

~~Figure 7c-e~~Note that Fig. 7b only presents the overall trends in flooding mechanisms at the continental scale, while disparate trends may exist in different regions that could cancel each other out. Therefore, we further ~~examines~~examined the trends in different event-based mechanisms in the 846 catchments~~,~~ (Figs. 7c–e), with the color representing the Theil-Sen slopes computed on the time series of respective proportions in individual catchments. ~~The proportion series were calculated using a 20-year moving window, where the 20-year time frame was used to ensure an adequate sample size for reliably estimating the intra-period proportions and also to guarantee enough periods to observe decadal variability . Only proportions that were~~

510 ~~calculated with at least 10 years of peak discharge data in each window were used to estimate the slope. The circular markers with black edges in the maps denote catchments with significant trends (α=0.05).~~ The results indicate that most catchments in the Alps, which are typically dominated by snowmelt, have experienced significant decreases in snowmelt-driven floods, while similar cases have occurred in Scandinavia as well (Fig. 7c). In contrast, extreme precipitation has become a more frequent cause of annual maximum discharges in the Massif Central, North European Plain, and the Alps, while decreased trends are

515 observed in some regions of Western Europe and especially southeast England (Fig. 7d). As for soil moisture-induced floods, their proportion generally shows opposing trends relative to those of extreme precipitation (Fig. 7e).

The decreasing trend in snowmelt-driven floods was also detected by Kemter et al. (2020), with 1.65% per decade, mainly occurring in eastern Europe, which was outside of our study area. In addition, they detected an increase in stratiform rainfall-

520 driven floods (0.49% per decade) mainly along the Mediterranean coast and an increase in soil moisture excess-driven floods (1.55% per decade) in the British Isles and central and northern Europe. The difference between Kemter et al. (2020) and this study probably arises from the varying study areas (the former additionally includes a large number of eastern and southern European catchments), as well as the definition of flood types. For example, their study defined soil moisture excess-driven floods as non-snowmelt floods when the mean soil water content was above 70% before a time window, and the remainder

525 were stratiform rainfall-driven floods. In contrast, this study used cluster analysis for the actual contributions of precipitation events before floods, and soil moisture-induced floods were related to annual maximum peak discharges where the contribution from antecedent precipitation is more important than recent precipitation.

3.~~5~~6 Possible causes and implications of the trends

To gain insights into the causes of the identified trends, we analyze five selected regions highlighted in Figs. 7c–e (see region

530 numbers in panel c), which feature consistent trends in certain mechanisms. For region 1 (the Alps) and region 3 (northeast Scandinavia), catchments with significant decreasing trends in snowmelt-driven events were considered. For region 2 (southeast France) and region 4 (northern Germany), we considered catchments with significant increasing trends in extreme precipitation-driven events, as well as those presenting significant decreases for region 5 (southeast England). Figure 8 shows the temporal regional evolution of the event-level mechanisms within the considered catchments, along with the change in

535 magnitude of the annual maximum 7-day ~~total~~ precipitation and mean spring temperatures ~~(January to April)~~ over the past 70 years. For the two regions with significant soil moisture effect on flooding (i.e., regions 4 and 5), we additionally added the averaged trends of ~~30-day precipitation preceding the 7-day window of recent precipitation for analysis, which is a common proxy for soil moisture prior to flooding . The time series of proportions were calculated by applying the previously described 20-year moving window to peak discharge classifications for the considered catchments. The annual precipitation extremes~~

540 ~~and mean spring temperatures were averaged across the catchments and then smoothed by using a 20-year moving average window for better visualization of their trends~~antecedent soil moisture conditions prior to flooding for analysis.
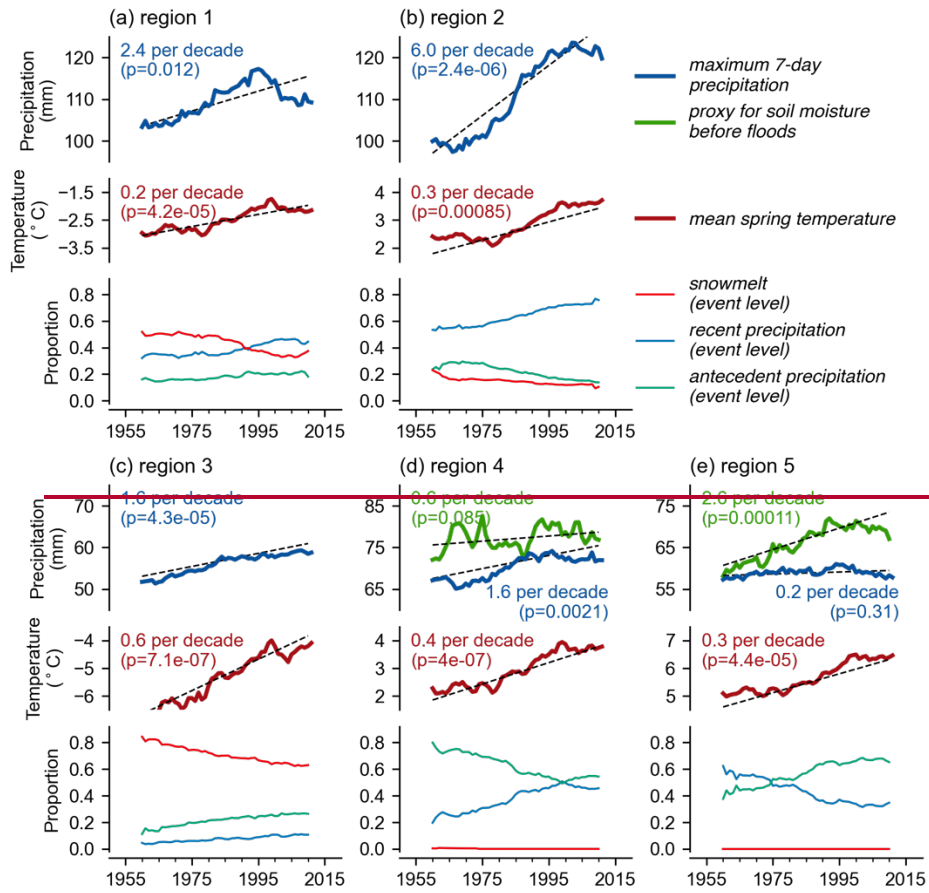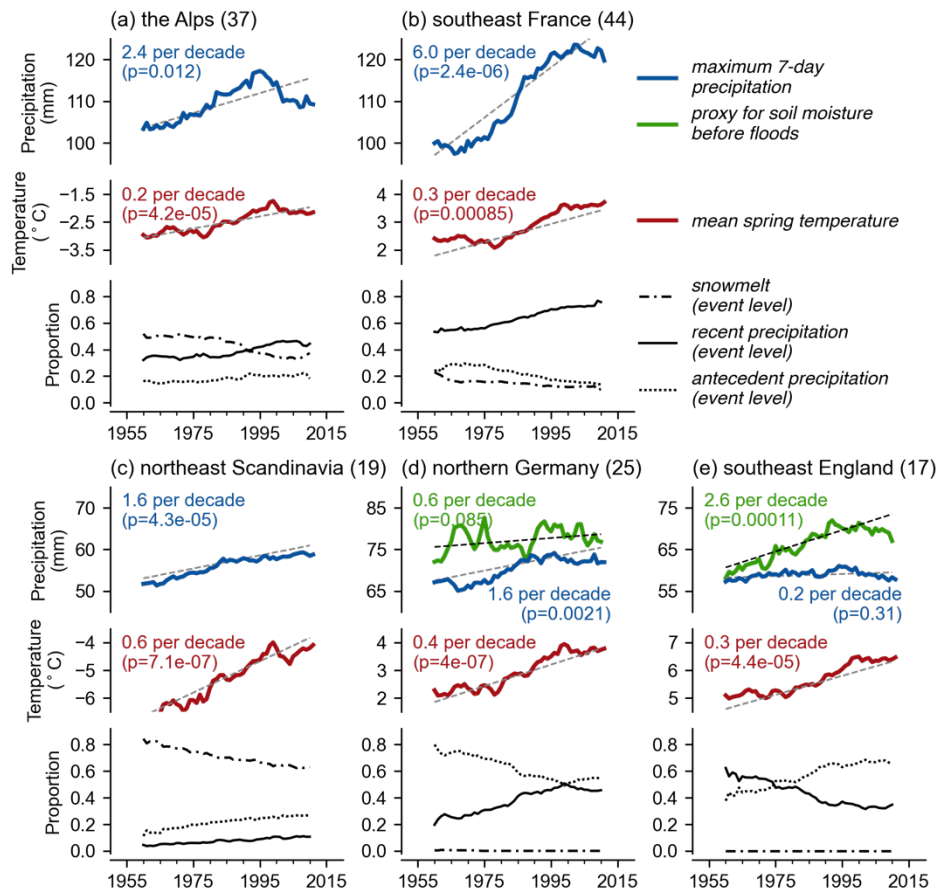
Figure 8: The temporal changes of the event-level mechanisms in relevant catchments within the five selected regions (see Fig. 7c), as well as the changes in average extreme precipitation (represented by annual maximum 7-day total precipitation), mean spring temperatures (represented by average temperature between January and April), and antecedent soil moisture conditions prior to flooding (represented by the 30-day total precipitation preceding the 7-day window of recent precipitation). The numbers in panel titles indicate the number of catchments considered. The proportions were calculated by a 20-year moving window, while precipitation and temperature were smoothed by using a 20-year moving average window~, with their values at central positions in time windows. The dashed black lines indicate the slope of relevant trends ~estimated by Theil-Sen's Estimator,~ with their significance being assessed by the modified Mann-Kendall test.

Mean spring temperatures have increased significantly in all five regions (Fig. 8), confirming the previous explanations for the reduced influence of snowmelt on river discharge annual maxima in snowy areas (regions 1-3) (Beniston and Stoffel, 2016; Vormoor et al., 2016). Furthermore, in regions 1–4, the increased magnitude of maximum 7-day precipitation can explain the rise in proportions of annual maximum peak discharges driven by extreme precipitation events. In contrast, the maximum 7-day precipitation in ~southern~southeast England (region 5) remained almost unchanged (Fig. 8e). Nonetheless, soil moisture conditions before discharges might have increased in ~southern~southeast England, as indicated by the increasing antecedent precipitation accumulations, which causes annual maximum discharge there to be more likely driven by soil moisture excesses

than by recent precipitation. Blöschl et al. (2017) stated that the region has a large subsurface water storage capacity, which is capable of storing a large amount of water that continuously increases until flooding occurs. In comparison, in northern Germany (region 4), the antecedent precipitation before annual maximum peak discharges has increased more slightly (Fig. 8d), while the increase in precipitation extremes likely caused an increase in floods driven by recent heavy precipitation. Note that here we merely examined the monotonic trends within data over the 70 years, while the trends may vary piecewise (e.g., the changes in maximum weekly precipitation in the Alps and southeast France), the impact of which on flooding mechanisms deserves further research.

A change in flooding mechanisms may affect the seasonality and magnitude of flooding, which might ultimately impair the current flood risk management measures. For example, in catchments previously dominated by snowmelt, ~~the seasonal patterns of flooding could change due to increasing floods from extreme precipitation and soil moisture excess. The case can be illustrated by using the circular statistics of the flood dates in catchments with a significant reduction of snowmelt-driven floods, such as some catchments in the Alps (region 1 in Fig. 7c). For the 37 catchments in the region, the overall proportion of annual maximum discharges caused by snowmelt has decreased from 50.2% in 1950–1985 to 37.6% in 1985–2020. Figures 9a and 9b compare changes in flood mean date and the corresponding mean resultant length at individual catchments, for snowmelt-driven floods and all floods irrespective of their cause, respectively. The resultant length is a measure between 0 and 1 that reflects the spread of a circular variable, with 0 representing the spread of flood dates evenly distributed over the year and 1 representing the spread concentrated at one day. It can be deducted from Fig. 9a that following the temperature increase, snowmelt-driven floods generally occur earlier in the year during 1985–2020 compared to 1950–1985, with a median shift of -3.8 days. On the other hand, annual peak discharges occur later in more than half of the catchments due to the increasing presence of other types of floods. Furthermore, Fig. 9b shows that the seasonality of annual maximum discharges has become more diffuse (decreasing mean resultant length) in most catchments for the same reason, though snowmelt-driven floods remain relatively stable.~~increasing floods from extreme precipitation and soil moisture excess may lead to shifted flood mean dates and less concentrated seasonal patterns (as exemplified in Fig. B1 in Appendix B). By simulating daily discharge for a reference period (1961–1990) and a future period (2071–2099), Vormoor et al. (2015) predicted that floods in some Nordic catchments could even shift from spring to autumn as rain replaced snowmelt as the dominant flood-inducing process. These results suggest that, in a warmer climate, flood risk predictions in snowmelt-affected catchments should consider the interconnection between changes in flooding drivers and seasonality.
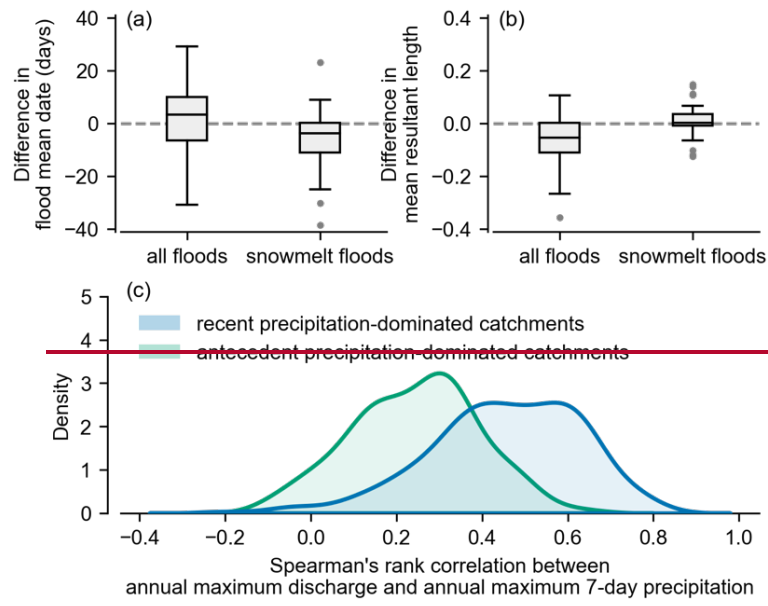
595

~~Although~~As for the impact on flooding magnitude, while it is challenging to link observed changes in individual flooding drivers alone to changes in flooding magnitudes, a link may appear especially in light of climate change (Blöschl et al., 2019).

600 For example, ~~Fig. 9c shows the distribution of Spearman's correlations between annual maximum discharge and annual maximum 7-day extreme precipitations for two groups of catchments, i.e., for recent precipitation-dominated catchments and antecedent precipitation-dominated catchments (based on Fig. 6a). Unsurprisingly,~~ the catchments where floods are dominated by recent precipitation tend to ~~have higher correlations than antecedent precipitation-dominated catchments, which indicates that the former might~~ be more susceptible to changes in extreme 7-day precipitation~~.~~ (Fig. B2 in Appendix B). Despite a lack

605 of sufficient observational evidence that the magnitude of floods increases with more extreme precipitation (Sharma et al., 2018), the trend of which is often determined jointly by both changes in rainfall and changes in antecedent soil moisture, some studies demonstrated the changed precipitation severity could vary the relationship between precipitation and streamflow (Bennett et al., 2018). When recent rainfall increases, changes in antecedent moisture conditions would become less important in modulating the response to rainfall (Wasko and Nathan, 2019). Brunner et al. (2021) indicated that it is possible to identify

610 a catchment-specific extremeness threshold, above which precipitation increases clearly produce greater flood magnitudes, and below which flood magnitude is strongly modulated by soil moisture. Therefore, the persistent risk that recent extreme precipitation would have an increasingly decisive role in flood generation for a large proportion of catchments, as implied by

Figure Fig. 7, cannot be disregarded. Recognizing the impact of such mechanism shifts in flooding mechanisms is crucial for understanding the link between changes in precipitation and flood risk in a warming climate.

3.7 Limitations and outlooks

In this study, we trained LSTM models individually for each catchment, while some studies have suggested that training a regional model for all catchments at once may be a better practice (e.g., Nearing et al., 2021). In the latter case, both meteorological time series and static catchment attributes are used as inputs to distinguish response behaviors across time and space, with the benefit that the ML model can learn more general relationships from a larger sample of hydrological variability (Kratzert et al., 2019b). However, introducing catchment attributes may prevent the identification of flood generation mechanisms based on distinguishable patterns of meteorological variables' contributions, which is the main objective of this study. Interpreting flooding mechanisms with regional LSTM models may become more challenging than with local LSTM models that use only meteorological time series, since some catchment attributes would confound the interpretation. Therefore, here we employed local models. Nevertheless, we note that using regional models can provide insight into how flooding mechanisms vary spatially, particularly for how the spatial distribution is affected by the geographic and climatic characteristics of catchments, and it merits more exploration in future studies.

Moreover, to strike the balance between model interpretability and accuracy, we only selected daily precipitation, temperature, and day length as meteorological inputs. The combination of inputs results in uncovering three well-known flooding mechanisms, which allows us to make a direct comparison with findings from other studies that used classical methods. However, with more input variables incorporated into the model, the methodology may be able to recognize more distinct patterns in terms of input contributions. In principle, this could allow identifying flooding mechanisms that are often overlooked and may not be easily explainable with well-known processes. However, it would likely be much more challenging to make sense of the flooding mechanisms from the likely much more complicated patterns in input feature importance, which we leave for future studies.

In the clustering procedure, we chose to use a 7-day window to aggregate the daily IG scores into a low-dimensional contribution vector for the sake of efficiency in clustering lengthy time series, which could induce inevitable uncertainties and subjectivity. Despite this, additional tests indicate that our findings are similar when using a 5-day window, which is also a common interval to consider flooding drivers (e.g., Rottler et al., 2021). Specifically, based on the 5-day window, the events identified with snowmelt, recent precipitation, or antecedent precipitation as the primary causes account for 15.0%, 47.9%, and 37.1% of all the 55,828 annual maximum peak discharges, which is only slightly different from using a 7-day window. As for the three mechanisms in individual catchments, decreasing the window length has the least impact on identifying snowmelt-driven floods, with the absolute changes in their proportions within 1% for 84.5% of catchments and within 5% for 98.7% of catchments. In comparison, the proportion changes for two other flooding types are more sensitive, with changes

within 5% for 83.2% (82.7%) of catchments in terms of recent (antecedent) precipitation-driven flooding. However, this does not affect the conclusion regarding the respective trends in flooding mechanisms (see Fig. S4 in the Supplementary Material), indicating the robustness of the methodology. Despite this sensitivity analysis, we would like to emphasize that the selection of the separating window remains somewhat subjective, and further exploration is needed to avoid a possible bias due to arbitrary judgments in identifying flooding mechanisms.

4 Conclusions

Flooding in rivers is usually caused by complex interactions between heavy precipitation, high soil moisture, and melting snow. Climate change has resulted in an overall decreased snowpack and more intense short-term precipitation extremes, which might systematically alter the interaction between flood drivers at the catchment level. Nevertheless, few studies have been able to To investigate whether flooding mechanisms have changed in European catchments, this study introduced a novel explainable ML method to identify a consistent continental scale climatic change signal in flooding mechanisms in Europe. Identifying such trends often requires a robust event based analysis, whereas the flooding mechanisms. Compared with conventional classification approach is highlyapproaches, where the results are usually dependent on appropriate flood process definitions and sensitive to changes in the subjectively designedthe selected indicators and threshold parameters. In this study, a, the combination of explainable ML and cluster analysis was used to identify different flooding mechanisms by grouping floods with similar patterns of is able to avoid such predefinitions and reduces subjectivities in identification processes. With the ML-captured feature importance of precipitation, temperature, and day length for predicting annual maximum discharges, we aggregated driver contributions. in the recent 7 days and an earlier period (back to 180 days) and then applied cluster analysis to group them based on similar patterns. As a result, the method identifies three major patterns that induce floods across 1,009 European catchments, corresponding to three typical flooding mechanisms, including recent precipitation (responsible for 48.3% of the annual maximum discharge events), antecedent precipitation (i.e., excessive soil moisture, accounting for 36.5%), and snowmelt (15.2%). The results indicate that for 25.6% of catchments, recent precipitation is the typical main contributor to floods, while floods are typically controlled by antecedent precipitation (linked to excessive soil moisture) in 12.3% of catchments. In around one-third (33.2%) of catchments, floods are dominated by a combination of recent heavy precipitation and antecedent precipitation events. It means, meaning that some floods there were caused by recent rains, and others were primarily driven by antecedent precipitation, although many of them were likely due to the compound effect between the two drivers. The remaining catchments are dominated by snowmelt (9.3%), or by combinations of snowmelt with the other two drivers. The spatial distribution of the dominant flooding mechanisms reflects the variation of the catchment's geographic and climatic characteristics and is generally consistent with results reported in earlier studies, some of which were obtained taking a perspective on catchment averagesdid not perform event-based classifications but rather identified the overall mechanisms within individual catchments.

We further detected changes in dominant flooding mechanisms over the last 70 years in over 18% of European catchments, especially some catchments that were previously dominated by single mechanisms became dominated by ~~mixed~~a mixture of mechanisms and some catchments show opposite shifts. Despite no regime shift from one single flooding mechanism to another single one, tendencies in their mechanisms at event levels were found. Specifically, when taking all annual maximum discharge events into account, those triggered by snowmelt have significantly decreased, with their proportion dropping by 0.7% per decade. Recent 7-day precipitation, on the other hand, has become increasingly important for flooding, with flooding triggered by such recent heavy precipitation increasing by 1.0% per decade. The changes in flooding mechanisms present a largely consistent pattern with climate change responses, and ~~the study highlights~~we discuss the potential risks associated with the resulting effects on flooding seasonality and magnitude.

Overall, ~~the identified changes in flooding mechanisms can provide important insights into understanding the effects of climate changes in the Earth system on flood events. Due to the compounding effect of various flooding drivers, it is generally challenging to establish a direct link between increases in extreme precipitation and increases in flood magnitudes. However, we find that as a consequence of extreme precipitation increases, recent precipitation has been more frequently observed as the primary cause of annual river discharge extremes. More research is required to investigate whether continually increasing extreme precipitation produces increased flood magnitudes, in particular after it overwhelmed the role of soil moisture in modulating flood events. Overall, our~~this study highlights the usability of explainable ML in helping uncover complex and possibly non-linear changes in weather and climate extreme events in the warming Earth system. With more large-sample hydrometeorological datasets becoming readily accessible, one next step is to extend the research to a larger scale for a better understanding of variations in flooding mechanisms globally. Still, many challenges remain for future work, providing potential research opportunities. For example, the clustering procedure can be improved by developing algorithms to aggregate daily feature importance adaptively, thereby avoiding the predefined separation window while maintaining high efficiency. Moreover, regional LSTM models that incorporate static catchment attributes can be employed to capture the spatial variations in flooding mechanisms and quantify the influence of catchments' geographical and climatic conditions on flooding processes. In addition to the integrated gradient method used in this study, other interpretation techniques might be explored further to uncover potentially valuable information when more input variables are included.

Appendix A
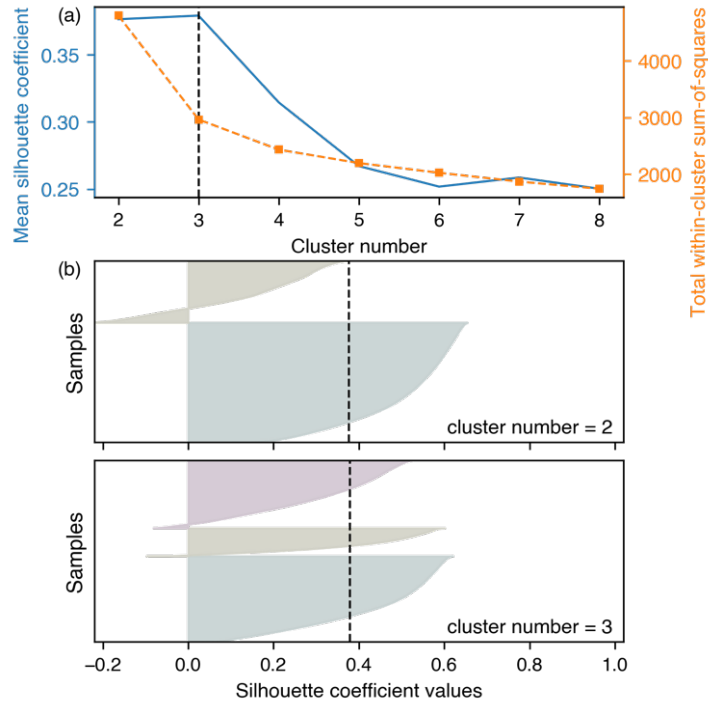
705

Figure A1: Determination of optimal cluster number. (a) The average silhouette coefficients and total within-cluster sum-of-squares assessed for respective candidate cluster numbers. (b) The silhouette plots for various clusters when the cluster number being 2 or 3, where the x-axis represents the silhouette coefficient for individual samples, and they were ordered by the coefficients and grouped by clusters in the y-axis. (a) suggests that clustering the samples into either two or three groups can achieve the similarly highest
710 **average silhouette coefficients, while the silhouette plots for individual samples under the two candidate numbers in (b) further suggest that clustering into three groups would be the best choice because a cluster with all below-average silhouette coefficients is present when clustering into two groups. Therefore, we cluster annual maximum peak discharges into three main groups in the main text.**

Appendix B
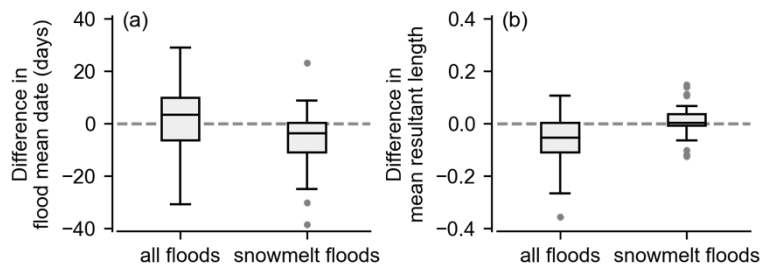
715

Figure B1: (a) Change in flooding mean dates (difference from 1985–2020 to 1950–1985) in 37 catchments with a significant reduction of snowmelt-driven floods in the Alps (region 1 in Fig. 7c) for snowmelt-driven floods and all floods irrespective of their cause. For these catchments, the overall proportion of annual maximum discharges caused by snowmelt has decreased from 50.2%

in 1950–1985 to 37.6% in 1985–2020. (b) The differences in mean resultant length of flood dates for the same cases as in (a). The mean resultant length is a measure in circular statistics between 0 and 1 that reflects the spread of a circular variable, with 0 representing the spread of flood dates evenly distributed over the year and 1 representing the spread concentrated at one day. It can be deducted from (a) that following the temperature increase, snowmelt-driven floods generally occur earlier in the year during 1985–2020 compared to 1950–1985, with a median shift of -3.8 days. On the other hand, annual peak discharges occur later in more than half of the catchments due to the increasing presence of other types of floods. Furthermore, (b) shows that the seasonality of annual maximum discharges has become more diffuse (decreasing mean resultant length) in most catchments for the same reason, though snowmelt-driven floods remain relatively stable.
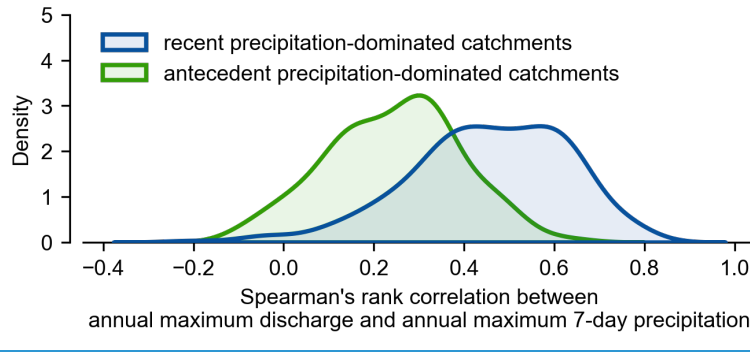
Figure B2: The distribution of Spearman's correlations between annual maximum discharge and annual maximum 7-day precipitation for two groups of catchments (blue, recent precipitation-dominated catchments; green, antecedent precipitation-dominated catchments, based on Fig. 6a). It shows that the catchments where floods are dominated by recent precipitation tend to have higher correlations than antecedent precipitation-dominated catchments, which implies that the former might be more susceptible to changes in extreme 7-day precipitation.

Data and code availability

The river discharge data can be obtained from the GRDC dataset (https://www.bafg.de/GRDC). The E-OBS gridded precipitation and temperature dataset is available at https://www.ecad.eu/download/ensembles/download.php(Haylock et al., 2008). Catchment attributes and boundaries are available at https://doi.pangaea.de/10.1594/PANGAEA.887477 (Do et al., 2018) and https://www.bafg.de/GRDC/EN/02_srvcs/22_gslrs/222_WSB/watershedBoundaries.html (Lehner, 2012). The 30 arc-second elevation data shown in Fig. 1a is accessible at http://doi.org/10.5066/F7DF6PQS. The code for the explainable machine learning framework is available at https://doi.org/10.5281/zenodo.4686106.

Author contribution

SJ and JZ conceived the study. SJ performed all analyses and wrote the initial draft. All authors substantially contributed to the final draft.

Competing interests

The authors declare that they have no conflict of interest.

Acknowledgements

The authors acknowledge the European COST Action DAMOCLES (CA17109) and the Helmholtz Initiative and Networking Fund (Young Investigator Group COMPOUNDX; grant agreement no. VH-NG-1537). This project has received funding from the European Union's Horizon 2020 research and innovation programme under grant agreement No 101003469 (XAIDA). We would like to acknowledge the use of the computing resources provided by Dr. Yi Zheng and thank Peter Miersch for proofreading the manuscript.

References

Alfieri, L., Burek, P., Feyen, L., and Forzieri, G.: Global warming increases the frequency of river floods in Europe, Hydrology and Earth System Sciences, 19, 2247-2260, https://doi.org/10.5194/hess-19-2247-2015, 2015.

Alfieri, L., Bisselink, B., Dottori, F., Naumann, G., de Roo, A., Salamon, P., Wyser, K., and Feyen, L.: Global projections of river flood risk in a warmer world, Earths Future, 5, 171-182, https://doi.org/10.1002/2016ef000485, 2017.

Barnes, E. A., Toms, B., Hurrell, J. W., Ebert-Uphoff, I., Anderson, C., and Anderson, D.: Indicator patterns of forced change learned by an artificial neural network, Journal of Advances in Modeling Earth Systems, 12, https://doi.org/10.1029/2020ms002195, 2020.

Bengtsson, L., Hodges, K. I., and Roeckner, E.: Storm tracks and climate change, Journal of Climate, 19, 3518-3543, https://doi.org/10.1175/jcli3815.1, 2006.

Beniston, M. and Stoffel, M.: Rain-on-snow events, floods and climate change in the Alps: Events may increase with warming up to 4 degrees C and decrease thereafter, Science of the Total Environment, 571, 228-236, https://doi.org/10.1016/j.scitotenv.2016.07.146, 2016.

Bennett, B., Leonard, M., Deng, Y., and Westra, S.: An empirical investigation into the effect of antecedent precipitation on flood volume, Journal of Hydrology, 567, 435-445, https://doi.org/10.1016/j.jhydrol.2018.10.025, 2018.

Berghuijs, W. R., Woods, R. A., Hutton, C. J., and Sivapalan, M.: Dominant flood generating mechanisms across the United States, Geophysical Research Letters, 43, 4382–4390, https://doi.org/10.1002/2016gl068070, 2016.

Berghuijs, W. R., Harrigan, S., Molnar, P., Slater, L. J., and Kirchner, J. W.: The relative importance of different flood-generating mechanisms across Europe, Water Resources Research, 55, 4582–4593, https://doi.org/10.1029/2019wr024841, 2019.

Bertola, M., Viglione, A., Lun, D., Hall, J., and Blöschl, G.: Flood trends in Europe: are changes in small and big floods different?, Hydrology and Earth System Sciences, 24, 1805-1822, https://doi.org/10.5194/hess-24-1805-2020, 2020.

Bertola, M., Viglione, A., Vorogushyn, S., Lun, D., Merz, B., and Bloeschl, G.: Do small and large floods have the same drivers of change? A regional attribution analysis in Europe, Hydrology and Earth System Sciences, 25, 1347-1364, https://doi.org/10.5194/hess-25-1347-2021, 2021.

Bevacqua, E., De Michele, C., Manning, C., Couasnon, A., Ribeiro, A. F. S., Ramos, A. M., Vignotto, E., Bastos, A., Blesic, S., Durante, F., Hillier, J., Oliveira, S. C., Pinto, J. G., Ragno, E., Rivoire, P., Saunders, K., van der Wiel, K., Wu, W. Y., Zhang, T. Y., and Zscheischler, J.: Guidelines for studying diverse types of compound weather and climate events, Earths Future, 9, https://doi.org/10.1029/2021ef002340, 2021.

780   Blanchet, J. and Creutin, J. D.: Co-occurrence of extreme daily rainfall in the French mediterranean region, Water Resources Research, 53, 9330-9349, https://doi.org/10.1002/2017wr020717, 2017.

Blöschl, G., Hall, J., Parajka, J., Perdigao, R. A. P., Merz, B., Arheimer, B., Aronica, G. T., Bilibashi, A., Bonacci, O., Borga, M., Canjevac, I., Castellarin, A., Chirico, G. B., Claps, P., Fiala, K., Frolova, N., Gorbachova, L., Gul, A., Hannaford, J., Harrigan, S., Kireeva, M., Kiss, A., Kjeldsen, T. R., Kohnova, S., Koskela, J. J., Ledvinka, O., Macdonald, N.,
785   Mavrova-Guirguinova, M., Mediero, L., Merz, R., Molnar, P., Montanari, A., Murphy, C., Osuch, M., Ovcharuk, V., Radevski, I., Rogger, M., Salinas, J. L., Sauquet, E., Sraj, M., Szolgay, J., Viglione, A., Volpi, E., Wilson, D., Zaimi, K., and Zivkovic, N.: Changing climate shifts timing of European floods, Science, 357, 588-590, https://doi.org/10.1126/science.aan2506, 2017.

Blöschl, G., Hall, J., Viglione, A., Perdigao, R. A. P., Parajka, J., Merz, B., Lun, D., Arheimer, B., Aronica, G. T., Bilibashi,
790   A., Bohac, M., Bonacci, O., Borga, M., Canjevac, I., Castellarin, A., Chirico, G. B., Claps, P., Frolova, N., Ganora, D., Gorbachova, L., Gul, A., Hannaford, J., Harrigan, S., Kireeva, M., Kiss, A., Kjeldsen, T. R., Kohnova, S., Koskela, J. J., Ledvinka, O., Macdonald, N., Mavrova-Guirguinova, M., Mediero, L., Merz, R., Molnar, P., Montanari, A., Murphy, C., Osuch, M., Ovcharuk, V., Radevski, I., Salinas, J. L., Sauquet, E., Sraj, M., Szolgay, J., Volpi, E., Wilson, D., Zaimi, K., and Zivkovic, N.: Changing climate both increases and decreases European river floods, Nature, 573,
795   108-+, https://doi.org/10.1038/s41586-019-1495-6, 2019.

Brunner, M. I., Swain, D. L., Wood, R. R., Willkofer, F., Done, J. M., Gilleland, E., and Ludwig, R.: An extremeness threshold determines the regional response of floods to changes in rainfall extremes, Communications Earth & Environment, 2, https://doi.org/10.1038/s43247-021-00248-x, 2021.

Cohen, J., Ye, H. C., and Jones, J.: Trends and variability in rain-on-snow events, Geophysical Research Letters, 42, 7115-
800   7122, https://doi.org/10.1002/2015gl065320, 2015.

Davenport, F. V., Herrera-Estrada, J. E., Burke, M., and Diffenbaugh, N. S.: Flood size increases nonlinearly across the western United States in response to lower snow-precipitation ratios, Water Resources Research, 56, https://doi.org/10.1029/2019wr025571, 2020.

Do, H. X., Gudmundsson, L., Leonard, M., and Westra, S.: The Global Streamflow Indices and Metadata Archive (GSIM) -
805   Part 1: The production of a daily streamflow archive and metadata, Earth System Science Data, 10, https://doi.org/10.5194/essd-10-765-2018, 2018.

Fischer, E. M. and Knutti, R.: Observed heavy precipitation increase confirms theory and early models, Nat. Clim. Chang., 6, 986-+, https://doi.org/10.1038/nclimate3110, 2016.

Fontrodona-Bach, A., van der Schrier, G., Melsen, L. A., Tank, A., and Teuling, A. J.: Widespread and accelerated decrease

810   of observed mean and extreme snow depth over Europe, Geophysical Research Letters, 45, 12312-12319, https://doi.org/10.1029/2018gl079799, 2018.

Forsythe, W. C., Rykiel, E. J., Stahl, R. S., Wu, H. I., and Schoolfield, R. M.: A model comparison for daylength as a function of latitude and day of year, Ecological Modelling, 80, 87-95, https://doi.org/10.1016/0304-3800(94)00034-f, 1995.

Gers, F. A., Schmidhuber, J., and Cummins, F.: Learning to forget: continual prediction with LSTM, 1999 Ninth International

815   Conference on Artificial Neural Networks ICANN 99. (Conf. Publ. No. 470), 7-10 Sept. 1999, 850-855 vol.852, 10.1049/cp:19991218,

Gobiet, A., Kotlarski, S., Beniston, M., Heinrich, G., Rajczak, J., and Stoffel, M.: 21st century climate change in the European Alps-A review, Science of the Total Environment, 493, 1138-1151, https://doi.org/10.1016/j.scitotenv.2013.07.050, 2014.

820   Hall, J. and Blöschl, G.: Spatial patterns and characteristics of flood seasonality in Europe, Hydrology and Earth System Sciences, 22, 3883-3901, https://doi.org/10.5194/hess-22-3883-2018, 2018.

Hall, J., Arheimer, B., Borga, M., Brazdil, R., Claps, P., Kiss, A., Kjeldsen, T. R., Kriauciuniene, J., Kundzewicz, Z. W., Lang, M., Llasat, M. C., Macdonald, N., McIntyre, N., Mediero, L., Merz, B., Merz, R., Molnar, P., Montanari, A., Neuhold, C., Parajka, J., Perdigao, R. A. P., Plavcova, L., Rogger, M., Salinas, J. L., Sauquet, E., Schar, C., Szolgay, J.,

825   Viglione, A., and Bloschl, G.: Understanding flood regime changes in Europe: a state-of-the-art assessment, Hydrology and Earth System Sciences, 18, 2735-2772, https://doi.org/10.5194/hess-18-2735-2014, 2014.

Hallema, D. W., Moussa, R., Sun, G., and McNulty, S. G.: Surface storm flow prediction on hillslopes based on topography and hydrologic connectivity, Ecological Processes, 5, https://doi.org/10.1186/s13717-016-0057-1, 2016.

Hamed, K. H. and Rao, A. R.: A modified Mann-Kendall trend test for autocorrelated data, Journal of Hydrology, 204, 182-

830   196, https://doi.org/10.1016/s0022-1694(97)00125-x, 1998.

Hamon, W. R.: Estimating potential evapotranspiration, Journal of the Hydraulics Division, 87, 107-102, https://doi.org/10.1061/JYCEAJ.0000599, 1961.

Haylock, M. R., Hofstra, N., Tank, A., Klok, E. J., Jones, P. D., and New, M.: A European daily high-resolution gridded data set of surface temperature and precipitation for 1950-2006, Journal of Geophysical Research-Atmospheres, 113,

835   https://doi.org/10.1029/2008jd010201, 2008.

Hirabayashi, Y., Mahendran, R., Koirala, S., Konoshima, L., Yamazaki, D., Watanabe, S., Kim, H., and Kanae, S.: Global flood risk under climate change, Nat. Clim. Chang., 3, 816-821, https://doi.org/10.1038/nclimate1911, 2013.

Hochreiter, S. and Schmidhuber, J.: Long short-term memory, Neural Computation, 9, 1735-1780, https://doi.org/10.1162/neco.1997.9.8.1735, 1997.

840   Isotta, F. A., Frei, C., Weilguni, V., Tadic, M. P., Lassegues, P., Rudolf, B., Pavan, V., Cacciamani, C., Antolini, G., Ratto, S. M., Munari, M., Micheletti, S., Bonati, V., Lussana, C., Ronchi, C., Panettieri, E., Marigo, G., and Vertacnik, G.: The

climate of daily precipitation in the Alps: development and analysis of a high-resolution grid dataset from pan-Alpine rain-gauge data, International Journal of Climatology, 34, 1657-1675, https://doi.org/10.1002/joc.3794, 2014.

Jiang, S. J., Zheng, Y., Wang, C., and Babovic, V.: Uncovering flooding mechanisms across the contiguous United States through interpretive deep learning on representative catchments, Water Resources Research, 58, https://doi.org/10.1029/2021wr030185, 2022.

Keller, L., Rossler, O., Martius, O., and Weingartner, R.: Delineation of flood generating processes and their hydrological response, Hydrological Processes, 32, 228-240, https://doi.org/10.1002/hyp.11407, 2018.

Kemter, M., Merz, B., Marwan, N., Vorogushyn, S., and Bloeschl, G.: Joint trends in flood magnitudes and spatial extents across Europe, Geophysical Research Letters, 47, https://doi.org/10.1029/2020gl087464, 2020.

Kingma, D. P. and Ba, J.: Adam: A method for stochastic optimization, 3rd International Conference on Learning Representations, San Diego, May 7-9 2015, https://doi.org/10.48550/arXiv.1412.6980, 2015.

Kratzert, F., Herrnegger, M., Klotz, D., Hochreiter, S., and Klambauer, G.: NeuralHydrology – Interpreting LSTMs in Hydrology, in: Explainable AI: Interpreting, Explaining and Visualizing Deep Learning, edited by: Samek, W., Montavon, G., Vedaldi, A., Hansen, L. K., and Müller, K.-R., Springer International Publishing, Cham, 347-362, https://doi.org/10.1007/978-3-030-28954-6_19, 2019a.

Kratzert, F., Klotz, D., Brenner, C., Schulz, K., and Herrnegger, M.: Rainfall-runoff modelling using Long Short-Term Memory (LSTM) networks, Hydrology and Earth System Sciences, 22, 6005–6022, https://doi.org/10.5194/hess-22-6005-2018, 2018.

Kratzert, F., Klotz, D., Shalev, G., Klambauer, G., Hochreiter, S., and Nearing, G.: Towards learning universal, regional, and local hydrological behaviors via machine learning applied to large-sample datasets, Hydrology and Earth System Sciences, 23, 5089–5110, https://doi.org/10.5194/hess-23-5089-2019, 2019b.

Labe, Z. M. and Barnes, E. A.: Detecting climate signals using explainable AI With single-forcing large ensembles, Journal of Advances in Modeling Earth Systems, 13, https://doi.org/10.1029/2021ms002464, 2021.

Lavers, D. A. and Villarini, G.: The nexus between atmospheric rivers and extreme precipitation across Europe, Geophysical Research Letters, 40, 3259-3264, https://doi.org/10.1002/grl.50636, 2013.

Ledingham, J., Archer, D., Lewis, E., Fowler, H., and Kilsby, C.: Contrasting seasonality of storm rainfall and flood runoff in the UK and some implications for rainfall-runoff methods of flood estimation, Hydrology Research, 50, 1309-1323, https://doi.org/10.2166/nh.2019.040, 2019.

Lees, T., Buechel, M., Anderson, B., Slater, L., Reece, S., Coxon, G., and Dadson, S. J.: Benchmarking data-driven rainfall-runoff models in Great Britain: a comparison of long short-term memory (LSTM)-based models with four lumped conceptual models, Hydrology and Earth System Sciences, 25, 5517-5534, https://doi.org/10.5194/hess-25-5517-2021, 2021.

Lees, T., Reece, S., Kratzert, F., Klotz, D., Gauch, M., De Bruijn, J., Kumar Sahu, R., Greve, P., Slater, L., and Dadson, S. J.:
875   Hydrological concept formation inside long short-term memory (LSTM) networks, Hydrol. Earth Syst. Sci., 26, 3079-3101, https://doi.org/10.5194/hess-26-3079-2022, 2022.

Lehner, B.: Derivation of watershed boundaries for GRDC gauging stations based on the HydroSHEDS drainage network, Federal Institute of Hydrology (BfG), Koblenz, 18 pp., 2012.

Merz, B., Vorogushyn, S., Uhlemann, S., Delgado, J., and Hundecha, Y.: HESS Opinions 'More efforts and scientific rigour
880   are needed to attribute trends in flood time series', Hydrology and Earth System Sciences, 16, 1379-1387, https://doi.org/10.5194/hess-16-1379-2012, 2012.

Merz, B., Blöschl, G., Vorogushyn, S., Dottori, F., Aerts, J. C. J. H., Bates, P., Bertola, M., Kemter, M., Kreibich, H., Lall, U., and Macdonald, E.: Causes, impacts and patterns of disastrous river floods, Nature Reviews Earth & Environment, 2, 592-609, https://doi.org/10.1038/s43017-021-00195-3, 2021.

885 Merz, R. and Blöschl, G.: A process typology of regional floods, Water Resources Research, 39, https://doi.org/10.1029/2002wr001952, 2003.

Moriasi, D. N., Gitau, M. W., Pai, N., and Daggupati, P.: Hydrologic and water quality models: Performance measures and evaluation criteria, Transactions of the Asabe, 58, 1763-1785, 2015.

Murdoch, W. J., Singh, C., Kumbier, K., Abbasi-Asl, R., and Yu, B.: Definitions, methods, and applications in interpretable
890   machine learning, Proceedings of the National Academy of Sciences of the United States of America, 116, 22071-22080, https://doi.org/10.1073/pnas.1900654116, 2019.

Nash, J. E. and Sutcliffe, J. V.: River flow forecasting through conceptual models part I — A discussion of principles, Journal of Hydrology, 10, 282–290, https://doi.org/10.1016/0022-1694(70)90255-6, 1970.

Nearing, G. S., Kratzert, F., Sampson, A. K., Pelissier, C. S., Klotz, D., Frame, J. M., Prieto, C., and Gupta, H. V.: What Role
895   Does Hydrological Science Play in the Age of Machine Learning?, Water Resources Research, 57, https://doi.org/10.1029/2020wr028091, 2021.

Nied, M., Pardowitz, T., Nissen, K., Ulbrich, U., Hundecha, Y., and Merz, B.: On the relationship between hydro-meteorological patterns and flood types, Journal of Hydrology, 519, 3249-3262, https://doi.org/10.1016/j.jhydrol.2014.09.089, 2014.

900 Pagano, T. and Garen, D.: A recent increase in western US streamflow variability and persistence, Journal of Hydrometeorology, 6, 173-179, https://doi.org/10.1175/jhm410.1, 2005.

Reichstein, M., Camps-Valls, G., Stevens, B., Jung, M., Denzler, J., Carvalhais, N., and Prabhat: Deep learning and process understanding for data-driven Earth system science, Nature, 566, 195–204, https://doi.org/10.1038/s41586-019-0912-1, 2019.

905 Rottler, E., Bronstert, A., Burger, G., and Rakovec, O.: Projected changes in Rhine River flood seasonality under global warming, Hydrology and Earth System Sciences, 25, 2353-2371, https://doi.org/10.5194/hess-25-2353-2021, 2021.

Rousseeuw, P. J.: Silhouettes - A graphical aid to the interpretation and validation of cluster-analysis, Journal of Computational and Applied Mathematics, 20, 53-65, https://doi.org/10.1016/0377-0427(87)90125-7, 1987.

Salvador, S. and Chan, P.: Toward accurate dynamic time warping in linear time and space, Intell. Data Anal., 11, 561–580, https://doi.org/10.5555/1367985.1367993, 2007.

Schiemann, R., Vidale, P. L., Shaffrey, L. C., Johnson, S. J., Roberts, M. J., Demory, M. E., Mizielinski, M. S., and Strachan, J.: Mean and extreme precipitation over European river basins better simulated in a 25km AGCM, Hydrology and Earth System Sciences, 22, 3933-3950, https://doi.org/10.5194/hess-22-3933-2018, 2018.

Sharma, A., Wasko, C., and Lettenmaier, D. P.: If precipitation extremes are increasing, why aren't floods?, Water Resources Research, 54, 8545-8551, https://doi.org/10.1029/2018wr023749, 2018.

Shen, C. P.: A transdisciplinary review of deep learning research and its relevance for water resources scientists, Water Resources Research, 54, 8558–8593, https://doi.org/10.1029/2018wr022643, 2018.

Sherstinsky, A.: Fundamentals of Recurrent Neural Network (RNN) and Long Short-Term Memory (LSTM) network, Physica D-Nonlinear Phenomena, 404, https://doi.org/10.1016/j.physd.2019.132306, 2020.

Sikorska, A. E., Viviroli, D., and Seibert, J.: Flood-type classification in mountainous catchments using crisp and fuzzy decision trees, Water Resources Research, 51, 7959-7976, https://doi.org/10.1002/2015wr017326, 2015.

Stein, L., Pianosi, F., and Woods, R.: Event-based classification for global study of river flood generating processes, Hydrological Processes, 34, 1514-1529, https://doi.org/10.1002/hyp.13678, 2020.

Stein, L., Clark, M. P., Knoben, W. J. M., Pianosi, F., and Woods, R. A.: How do climate and catchment attributes influence flood generating processes? A large-sample study for 671 catchments across the contiguous USA, Water Resources Research, 57, 21, https://doi.org/10.1029/2020wr028300, 2021.

Su, Y. H. and Kuo, C. C. J.: On extended long short-term memory and dependent bidirectional recurrent neural network, Neurocomputing, 356, 151-161, https://doi.org/10.1016/j.neucom.2019.04.044, 2019.

Sundararajan, M., Taly, A., and Yan, Q.: Axiomatic attribution for deep networks, Proceedings of the 34th International Conference on Machine Learning, Sydney, Australia2017.

Tarasova, L., Basso, S., Wendi, D., Viglione, A., Kumar, R., and Merz, R.: A Process-Based Framework to Characterize and Classify Runoff Events: The Event Typology of Germany, Water Resources Research, 56, https://doi.org/10.1029/2019wr026951, 2020.

Tarasova, L., Merz, R., Kiss, A., Basso, S., Blöschl, G., Merz, B., Viglione, A., Plotner, S., Guse, B., Schumann, A., Fischer, S., Ahrens, B., Anwar, F., Bardossy, A., Buhler, P., Haberlandt, U., Kreibich, H., Krug, A., Lun, D., Muller-Thomy, H., Pidoto, R., Primo, C., Seidel, J., Vorogushyn, S., and Wietzke, L.: Causative classification of river flood events, Wiley Interdisciplinary Reviews-Water, 6, https://doi.org/10.1002/wat2.1353, 2019.

Tavenard, R., Faouzi , J., Vandewiele, G., Divo, F., Androz , G., Holtz, C., Payne, M., Yurchak, R., Rußwurm, M., Kolar, K., and Woods, E.: Tslearn, a machine learning toolkit for time series data, Journal of Machine Learning Research, 21, 1-6, 2020.

Tellman, B., Sullivan, J. A., Kuhn, C., Kettner, A. J., Doyle, C. S., Brakenridge, G. R., Erickson, T. A., and Slayback, D. A.: Satellite imaging reveals increased proportion of population exposed to floods, Nature, 596, 80-+, https://doi.org/10.1038/s41586-021-03695-w, 2021.

945 Toms, B. A., Barnes, E. A., and Ebert-Uphoff, I.: Physically interpretable neural networks for the geosciences: Applications to Earth system variability, Journal of Advances in Modeling Earth Systems, 12, https://doi.org/10.1029/2019ms002002, 2020.

Trenberth, K. E.: Changes in precipitation with climate change, Climate Research, 47, 123-138, https://doi.org/10.3354/cr00953, 2011.

Turkington, T., Breinl, K., Ettema, J., Alkema, D., and Jetten, V.: A new flood type classification method for use in climate
950 change impact studies, Weather and Climate Extremes, 14, 1-16, https://doi.org/10.1016/j.wace.2016.10.001, 2016.

Vormoor, K., Lawrence, D., Heistermann, M., and Bronstert, A.: Climate change impacts on the seasonality and generation processes of floods - projections and uncertainties for catchments with mixed snowmelt/rainfall regimes, Hydrology and Earth System Sciences, 19, 913-931, https://doi.org/10.5194/hess-19-913-2015, 2015.

Vormoor, K., Lawrence, D., Schlichting, L., Wilson, D., and Wong, W. K.: Evidence for changes in the magnitude and
955 frequency of observed rainfall vs. snowmelt driven floods in Norway, Journal of Hydrology, 538, 33-48, https://doi.org/10.1016/j.jhydrol.2016.03.066, 2016.

Wasko, C. and Nathan, R.: Influence of changes in rainfall and soil moisture on trends in flooding, Journal of Hydrology, 575, 432-441, https://doi.org/10.1016/j.jhydrol.2019.05.054, 2019.

Whan, K., Sillmann, J., Schaller, N., and Haarsma, R.: Future changes in atmospheric rivers and extreme precipitation in
960 Norway, Climate Dynamics, 54, 2071-2084, https://doi.org/10.1007/s00382-019-05099-z, 2020.

Yu, S. W. and Ma, J. W.: Deep learning for geophysics: Current and future trends, Reviews of Geophysics, 59, https://doi.org/10.1029/2021rg000742, 2021.

Zscheischler, J., Westra, S., van den Hurk, B., Seneviratne, S. I., Ward, P. J., Pitman, A., AghaKouchak, A., Bresch, D. N., Leonard, M., Wahl, T., and Zhang, X. B.: Future climate risk from compound events, Nat. Clim. Chang., 8, 469-477,
965 https://doi.org/10.1038/s41558-018-0156-3, 2018.

Zscheischler, J., Martius, O., Westra, S., Bevacqua, E., Raymond, C., Horton, R. M., van den Hurk, B., AghaKouchak, A., Jezequel, A., Mahecha, M. D., Maraun, D., Ramos, A. M., Ridder, N. N., Thiery, W., and Vignotto, E.: A typology of compound weather and climate events, Nature Reviews Earth & Environment, 1, 333-347, https://doi.org/10.1038/s43017-020-0060-z, 2020.

970